Advanced Devices & Instrumentation
A SCIENCE PARTNER JOURNAL

REVIEW ARTICLE

Understanding the Thermoelectric Transport Properties of Organic Semiconductors through the Perspective of Polarons

Deepak Venkateshvaran[1,2,3*], Mateo T. R. Cervantes[1,4], Leszek J. Spalek[1,2], Ki-Hwan Hwang[1,2], Kaspars Pudzs[5], Martins Rutkis[5*], Guillaume Schweicher[6], and Pablo Padilla-Longoria[4]

[1]Cavendish Laboratory, University of Cambridge, Cambridge CB3 0HE, UK. [2]Department of Chemical Engineering and Biotechnology, University of Cambridge, Cambridge CB3 0AS, UK. [3]Department for Science, Innovation and Technology (DSIT), UK Government, London SW1A 2BQ, UK. [4]IIMAS, Mathematics and Mechanics Department, Universidad Nacional Autonoma de México (UNAM), Ciudad Universitaria, México. [5]Institute of Solid State Physics, University of Latvia, Riga LV-1063, Latvia. [6]Laboratoire de Chimie des Polymères, Faculté des Sciences, Université Libre de Bruxelles (ULB), 1050 Brussels, Belgium.

*Address correspondence to: dv246@cam.ac.uk (D.V.); martins.rutkis@cfi.lu.lv (M.R.)

Citation: Venkateshvaran D, Cervantes MTR, Spalek LJ, Hwang KH, Pudzs K, Rutkis M, Schweicher G, Padilla-Longoria P. Understanding the Thermoelectric Transport Properties of Organic Semiconductors through the Perspective of Polarons. *Adv. Devices Instrum.* 2024;5:Article 0067. https://doi.org/10.34133/adi.0067

Submitted 11 June 2024
Revised 8 August 2024
Accepted 26 August 2024
Published 26 November 2024

Thermoelectric properties of organic semiconductors have been intensively studied over the last 15 years for their application in converting waste heat into electricity. Optimism in the field of organic thermoelectrics points at the possibility of achieving figures of merit (ZT) approaching or exceeding one. Despite tremendous research effort over the years, however, such market-competitive values of ZT have not been demonstrated. The efficiency of waste heat to electricity conversion using organic semiconductors depends on their transport physics. This physics is understood through the interrelationship between the electrical conductivity (σ), the Seebeck coefficient (S), and the thermal conductivity (κ). Several thermoelectric transport models were developed to explain the observed relationship between these coefficients in organic semiconductors. Most models predict the measured thermoelectric transport behavior within a limited range, either in the nondegenerate regime of low electrical conductivity or in the near-degenerate regime of high electrical conductivity. Here, we deploy a simple model based on hopping transport to explain the experimentally observed relationship between the electrical conductivity and the Seebeck coefficient in organic semiconductors. This hopping-based transport model spans a broad range of charge carrier densities encompassing both the nondegenerate regime and the near-degenerate regime. The model was originally used to identify polaronic transport in multifunctional conductive oxide-based materials and is shown here to be applicable to organic semiconductors. Our work spotlights an alternative explanation for recent experimental observations in organic thermoelectrics within a unified description. It documents factors that keep $ZT \sim 1$ elusive in single layers of organic semiconductors, despite their understood merits in thermoelectrics.

Introduction

Over the last few decades, organic semiconductors have enabled a revolution in flexible electronics. As a class of materials processed into functional devices from solution, they are an integral choice for applications in electronics and energy generation, which necessitate deployment over large areas. The deposition of organic semiconductors is done using low-cost fabrication routes such as inkjet printing, spray coating, screen printing, and 3-dimensional printing. These deposition routes remain distinct from those used to fabricate electronic devices from inorganic semiconductors. In addition, the multifunctional properties of organic semiconductors are tailorable through chemical design of their constituent molecular units. The unique ability to design organic semiconductors with optimized properties offers applications the added benefit of materials choice. The above are select attributes that preserve the relevance of organic semiconductors in emerging technological applications such as large-area thermoelectric waste heat harvesting.

Organic semiconductors are suited for thermoelectric applications owing to their low thermal conductivities (κ), relatively large and tunable Seebeck coefficients (S), and their ability to conduct charge carriers with reasonably high electrical conductivities (σ). Since the thermoelectric figure of merit is defined as $ZT = (S^2\sigma/\kappa)T$, an organic semiconductor having $\kappa = 0.3$ W m^{-1} K^{-1} and a power factor $S^2\sigma \sim 10^{-3}$ W m^{-1} K^{-2} should effortlessly demonstrate the benchmark figure in thermoelectrics of $ZT \sim 1$ at 300 K. Although these values of the power factor and the thermal conductivity are, independently, very much within the parameter space covered by organic semiconductors, they have

been difficult to achieve simultaneously. This difficulty has kept an unambiguous demonstration of $ZT \sim 1$ out of bounds. To gauge whether $ZT \sim 1$ is achievable using organic semiconductors, an in-depth understanding of the interrelationship between the electrical conductivity, the Seebeck coefficient, and the thermal conductivity within the parameter space covered by organic semiconductors is necessary. Several attempts have been made in the recent past to understand this interdependency, but a conclusive and universally accepted comprehension of the same is yet to emerge.

This review article is not written to purely summarize the various pieces of literature on organic thermoelectrics to describe the status quo. There are several articles that do such a task well. Rather, ours is written in a manner that attempts to piece together various prominent measurements of thermoelectric transport coefficients on organic semiconductors published in the literature. In adopting a broad perspective, and in prioritizing simplicity in modeling the observations, we attempt to show how the comprehensive landscape of measurements in the literature on organic thermoelectrics coherently points at the role of mobile polarons in carrier transport. Based on this inference, we estimate the intrinsic upper bound on ZT achievable within an organic semiconductor where rapid electronic transport is polaron mediated.

There is a pressing need for the observations in the literature on organic thermoelectrics to be coherently explained within a unified framework. It is preferable that such a framework be not overtly complex to deter one's visualization of the microscopic transport mechanisms at play. As of now, many of the observations in the literature have been explained using a combination of localized hopping transport and delocalized metallic transport together with transitions from one to the other upon increasing the density of charge carriers within the organic semiconductor. At times, the temperature-dependent electrical conductivity is explained using hopping models, but the accompanying temperature-dependent Seebeck coefficient in the same system is modeled based on the Mott formula for metals. This dissonance in the literature is addressed herein. We purport a view that organic semiconductors are intrinsically van der Waal's bonded materials that enable large effective mass polaronic charge transport within narrow bands. This view universally explains the observations and unites the nondegenerate regime with the near-degenerate regime using a single simplified transcendental equation connecting the Seebeck coefficient with the electrical conductivity.The structure of this review article is organized as follows. After a brief description of organic semiconductors, we summarize their Seebeck coefficient, and their electrical conductivity measured in 2 different transport regimes. The first regime is the nondegenerate regime of low electrical conductivity where the carrier density remains much smaller than the total number of available states that mediate their motion. The second regime is what we refer to as the near-degenerate regime of high electrical conductivity where the carrier density approaches the total number of available states. Once these observations have been highlighted, we describe the Jonker model that is routinely used in thermoelectrics to link the Seebeck coefficient with the carrier density in the nondegenerate regime. Upon introducing corrections to the Jonker model at high carrier densities to account for polaronic hopping within narrow bands, we show that this modified Jonker model replicates the salient features observed in the literature in a manner consistent over a broad range of electrical conductivities spanning both the nondegenerate regime and the near-degenerate regime. We discuss how temperature-dependent measurements of the electrical conductivity and the Seebeck coefficient in organic semiconductors are consistent with the modified Jonker model that supports the existence of polarons at large carrier densities. The exposition is wrapped up by highlighting alternative applications of organic thermoelectrics beyond power generation, in the case where polaronic transport in organic semiconductors becomes an intrinsic deterrent to achieving $ZT \sim 1$.

Organic Semiconductors: Structure, Disorder, and Carrier Transport

Organic semiconductors are macromolecular carbon-based systems in the form of polymers and small molecules. A few chemical structures of organic semiconductors are shown in Fig. 1. For ease of readability in this review article, these organic semiconductors will be referred to by the accompanying shorthand names shown in Fig. 1 rather than by their original elaborate chemical names. A distinguishing feature of these macromolecular systems is that they contain conjugated rings within their backbones leading to delocalized π electron clouds that envelope them. When packed in the solid state, the repulsion between π electron clouds of adjacent organic molecules keep them from collapsing on each other. The typical $\pi - \pi$ stacking distance is around 3.7 Å but can vary depending on extraneous molecular incorporation [1]. In organic films, long chains of repeated monomer units line up against each other to form ordered domains on the nanoscale or on the microscale depending on the extent of spatial ordering induced during self-assembly. Organic small molecules possess ordering over much larger length scales spanning entire crystals, millimeters in size.

The intrinsic nature of carrier transport within organic polymers and organic small molecules differs on account of the degree of carrier localization induced by the extent of disorder in the solid state. When talking of disorder in organic semiconductors, one normally refers to a combination of various contributions. On the microscale, morphological disorder is caused by the presence of grain boundaries within the solid state that impedes carrier motion through scattering. On the nanoscale, structural disorder could be caused in polymers by hairpin bends having high bending curvatures. In small molecules, it can be caused by a change in the relative orientation of a molecule within lattice packing. On the molecular scale, positional disorder could be caused by a misplacement of alkyl side chains from an expected packing motif. Also on the molecular scale, torsional disorder is caused in polymers having large twists within the polymer backbone due to rotations about single bonds. Energetic disorder refers to disruptions in the energetic landscape within which carriers move. It is indicated by how wide or how narrow the density of trap states is and bears contributions from the previously mentioned types of disorder. Dynamic disorder is seen in molecular semiconductors that are affected by thermal motion. It leads to dynamic variations in the spatial extent of the wavefunction of charge carriers, localizing them in transience.

From a measurement viewpoint, the combined extent of disorder is inferred from the magnitude of the charge carrier mobility (μ), its dependence on temperature, its modulation under applied electric fields (as in organic transistors), and its measurement under applied magnetic fields (as in the Hall effect and in magnetoconductance). Organic polymers typically

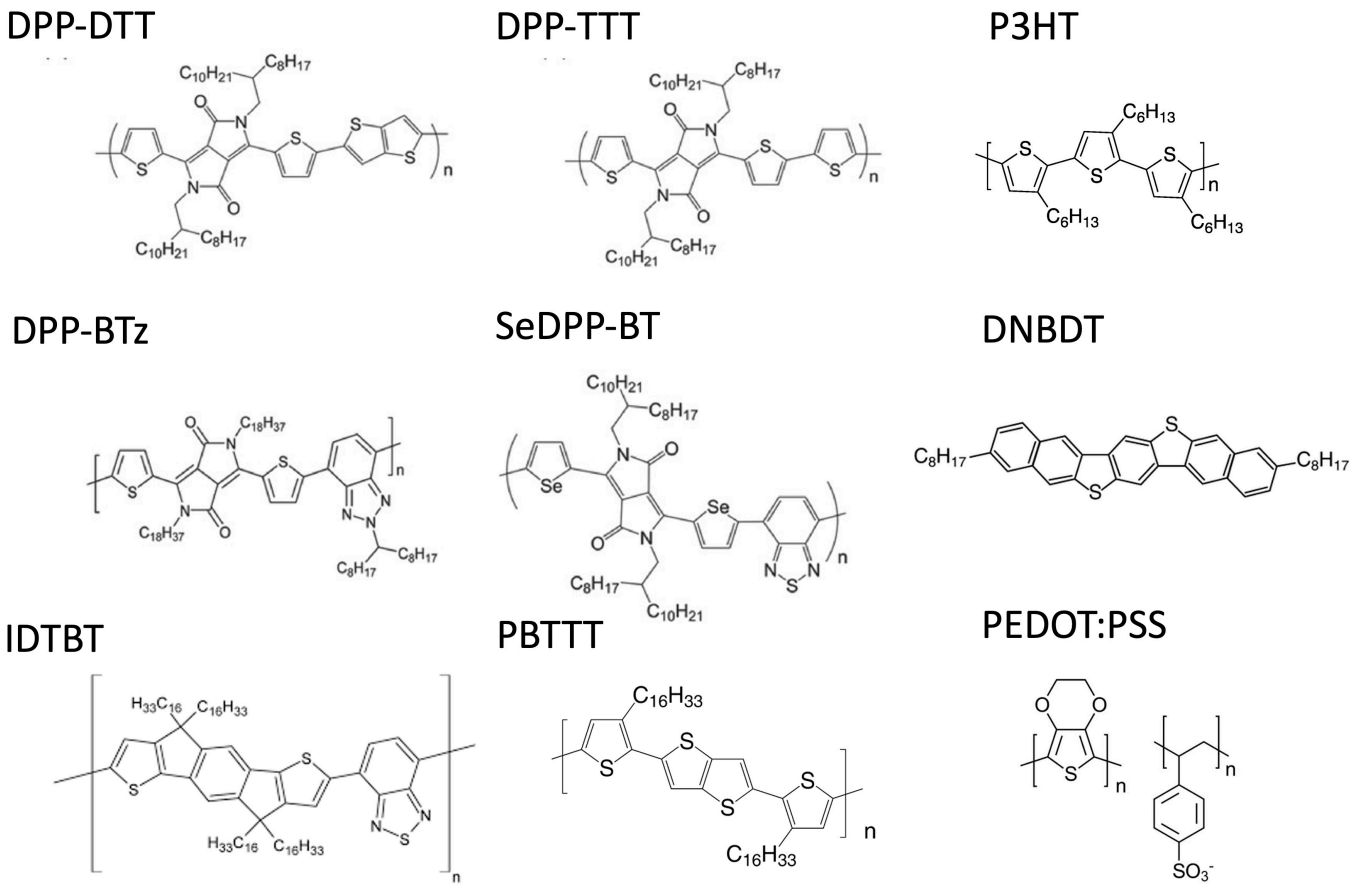

Fig. 1. Organic semiconductors. A selection of organic semiconductors used in electronics and thermoelectrics.

have carrier mobilities around 1 cm^2/Vs. Small molecules and molecular crystals have shown carrier mobilities in the tens of cm^2/Vs. The carrier density-dependent modulation of the Seebeck coefficient is another measurement using which disorder can be estimated [2–4].

Charge carriers are introduced into an organic semiconductor via injection from a metal electrode under the influence of an electric field across a solid-state dielectric layer. Such is the case in conventional polymer dielectric organic field effect transistors. They can also be induced using ionic gel gating where the capacitance of the mixed dielectric is 10 times larger than those used in conventional organic field effect transistors [5–7]. Ionic gel gating is thus an avenue to generate carrier densities 10 times larger than that of solid-state polymer dielectric-based organic transistors. In addition to gating, charge carriers can also be introduced through molecular doping, which involves having donor molecules infuse themselves into organic semiconductor matrices and donate charge carriers to their host [8]. Organic semiconductors are intrinsically nonconducting unless field effect gated or doped. This is because most carriers are localized in trap states within the density of states (DOS) that must first be filled before mobile states at higher energies can be accessed. Organic semiconductors only conduct charges that have been injected or introduced into them. They do not support minority carrier conduction. This limitation makes them operational only in a charge accumulation regime within field effect devices. They contrast inorganic semiconductor-based field effect devices in which conduction can operate in an inversion regime in addition to the accumulation regime.

Charge carriers within organic polymers travel via stochastic hopping down their molecular backbones or down their $\pi - \pi$ stacking directions. The alkyl side chains within organic polymers are useful in ensuring that they can be dissolved and processed from solution but are known to impede carrier transport owing to a lack of charge conjugation in them. Their presence causes organic polymers to display an anisotropy in carrier transport properties.

Disorder-induced charge localization causes a carrier's residence time to be sufficiently long to permit spatial polarization during transit. Hence, when charge carriers in organic semiconductors move, they drag along with them a cloud of polarization arising from a coulombic interaction with the molecule they skim over. These carriers therefore sport larger effective masses and lower mobilities compared to carriers in more crystalline inorganic semiconductors. The charge carriers accompanied by their polarization clouds are composite quasiparticles known as polarons [9–13]. The spatial extent to which they polarize their host medium renders them either small polarons or large polarons. There are reports on the existence of both small and large polarons in organic semiconductors depending on the extent of order and organization within the molecular lattice [14–20]. Large polarons have been observed in organic single-crystal transistors, with dielectric/organic interfaces having low interfacial polarization. In contrast to organic molecular crystals, organic polymers have a greater extent of energetic disorder, which stipulates greater spatial localization of charges. Their transport properties are known to be mediated by small polarons [12,21]. These polarons diffuse through the host organic

semiconductor under an external force influence of electric or magnetic fields, hopping from one available site to another. Polarons continue to exist in organic semiconductors upon doping [22–29].

Depending on the extent of disorder within the energetic landscape and depending on the energy level at which transport occurs within the DOS, charge carrier hopping takes place through either an adiabatic process or a nonadiabatic process [30]. Polaronic hopping between equivalent sites is typically adiabatic [12,31–33]. This is because the motion of polarons through an organic semiconductor necessitates the motion of a charge carrier together with its polarization cloud. This action cannot take place over a broad energetic range and is limited to a narrow range of energies, typically on the order of k_BT [12,34]. Governed by this stipulation of polaronic bands being narrow, and one where all the induced charges access all the available states for transport at a given temperature, transport in these systems is described as a function of the fractional occupancy of states, c [2,12,35,36]. The fractional occupancy refers to the ratio of carrier density n distributed over a given number of available states N. This description simplifies the mathematical formulation of the Seebeck coefficient in organic semiconductors, making it an argument of configurational entropy that depends solely on the fractional occupancy $c = \frac{n}{N}$. The conductivity in this scenario is a function of $c(1-c)$ and reflects the probability that carriers hop from a filled state into an available empty state [35]. The transport coefficients defined through fractional occupancies of polarons within narrow bands are a defining feature of organic semiconductors. The spatial extent of a small polaron is comparable to the lattice constant of the medium it moves through. In the case of polymers, this is the extent of a single monomer unit. For this reason, the total number of available states N can be computed as the inverse of the volume occupied by a single monomer unit. This number is typically around 10^{21} cm^{-3} available states [2].

In this work, we distinguish 2 regimes of carrier transport. The first is the nondegenerate regime where the number of induced charge carriers $n \ll N$. This is the regime covered by organic field effect transistors with conventional solid-state polymer dielectrics where n is tuned up to a maximum of a few 10^{19} cm^{-3}. The second is the near-degenerate transport regime where n exceeds 10^{20} cm^{-3} and begins to be comparable with N. This regime is covered by ionic gel-gated field effect transistors, molecularly doped organic semiconductors, and electrochemically doped organic semiconductors [5,28,37–40].

Thermoelectric Transport in Organic Polymers within the Nondegenerate Regime of Transport

Organic field effect devices that use polymeric dielectrics such as Cytop and poly(methyl methacrylate) (PMMA), hundreds of nanometers thick, achieve a maximum carrier density in the accumulation regime of a few 10^{19} cm^{-3}. While organic transistors have a large in-plane source–drain voltage that induces motion of charge carriers to generate a current, organic thermoelectric devices generate carrier flow from much smaller thermal gradient-induced potential differences. One such organic thermoelectric device is shown in Fig. 2A. A microfabricated stripe heater is lithographically patterned next to the source drain electrodes, and within 20 μm from one of them. The distance between the two 20-μm-wide source and drain electrodes is 50 μm and constitutes the channel of the device. An organic semiconductor (shown in purple) is patterned over the source drain micro-electrodes and is coated with a dielectric layer of either Cytop or PMMA having a thickness of approximately 500 nm. Over this dielectric layer, a metal gate electrode is deposited as shown in Fig. 2A. Such a

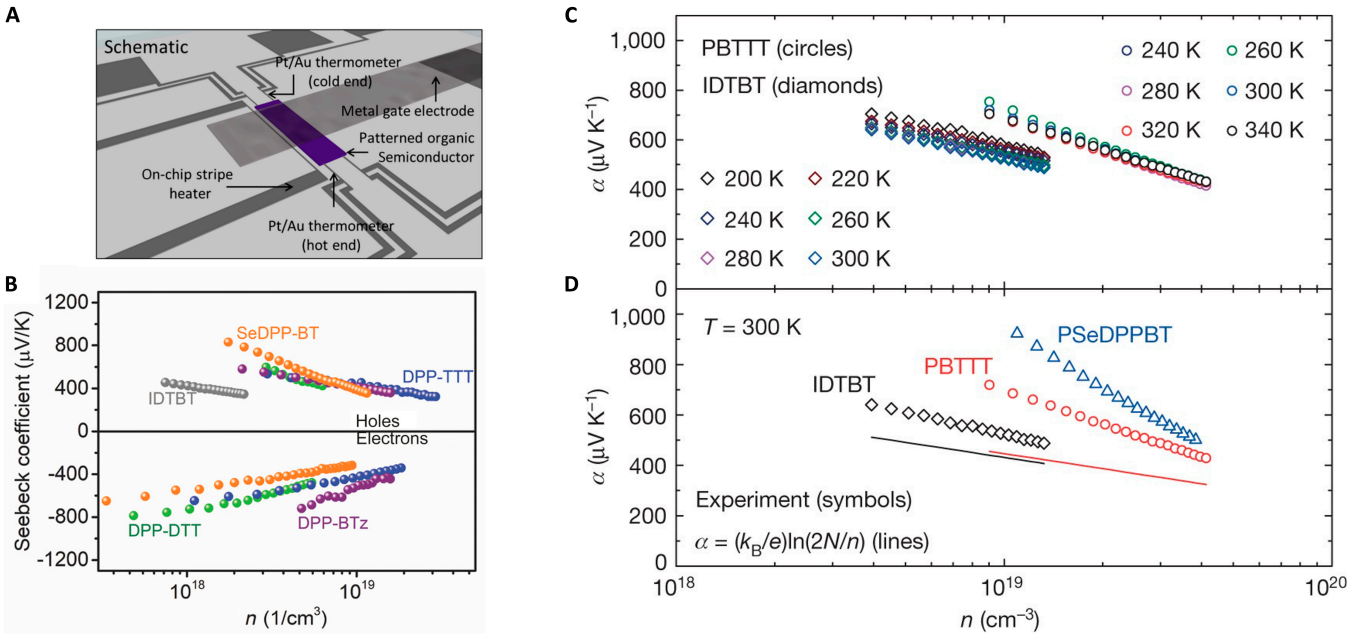

Fig. 2. Seebeck coefficient in organic polymers within the nondegenerate regime of transport. (A) Schematic of a field effect device in which gate voltage-modulated Seebeck coefficients are measured. (B) Seebeck coefficient as a function of carrier density for a variety of organic polymers that show ambipolar transport. (C) Temperature invariance of the Seebeck coefficient in organic polymers within the nondegenerate transport regime. (D) Voltage-modulated Seebeck coefficients in 3 well-known organic semiconductors compared to a model in which all induced carriers contribute to entropy transport. Image taken from [2,3].

device operates as an organic transistor when the microfabricated stripe heater is left switched off. When a current is run through the stripe heater, Joule heating causes it to dissipate heat into the substrate and into the rest of the device, generating a temperature difference between the source and drain electrodes. The temperature gradient is sustained by the glass substrate upon which the device is fabricated. This is because the low conductivity glass substrate is around 700 μm thick in comparison with the complete device stack, which, including all its constitutional layers, is less than 0.6 μm. Within such a device, the gate voltage is used to tune the carrier density in the channel, at the interface between the polymer dielectric and the organic semiconductor. Due to the applied in-plane temperature difference, a thermal voltage is generated between the source and drain electrodes, which sensitively depends on the electronic properties of the bridging organic semiconductor as well as the carrier density within it. For an on-chip stripe heater with a power dissipation of about 70 mW, the temperature difference generated between the source and drain electrodes 50 μm apart is around 2.5 K. The thermal voltage generated in the nondegenerate organic semiconductor is in the range of several hundreds of microvolts to a few millivolts. These are approximate values found in our devices. They will vary depending on the device geometry, thickness of the heater, the electrodes, and the thermal properties of the substrate.

The Seebeck coefficient is the ratio of the measured thermal voltage response to the applied temperature difference, i.e., α or $S = \frac{\Delta V}{\Delta T}$. The units of the Seebeck coefficient are thus $\frac{V}{K}$. The units of entropy on the other hand are $\frac{J}{K}$. This implies that the Seebeck coefficient is a measure of the entropy per unit charge carrier, since $\frac{V}{K}$ is $\frac{J}{K}/C$, where C is a Coulomb [12]. Thus, as the carrier density within the organic semiconductor is raised, the Seebeck coefficient is expected to reduce, because upon increasing the carrier density, there are more carriers that share in the entropy at the given temperature.

Figure 2B shows the Seebeck coefficient measured in a variety of ambipolar organic semiconductors based on diketopyrrolopyrrole (DPP) core motifs. The Seebeck coefficient is linear on a linear–log scale when plotted against carrier density n in this regime of nondegenerate transport where $n \ll N$. The slope of the Seebeck coefficient on this plot can be used as a comparison between the extent of disorder within the various polymers and as a comparison between the relative freedom of holes and electrons within the same polymer [3]. Figure 2C shows the temperature dependence of the Seebeck coefficient measured in 2 different polymers, PBTTT and IDTBT, within the nondegenerate transport regime [2]. Figure 2D maps the Seebeck coefficient of 3 organic polymers, PBTTT, PSeDPPBT, and IDTBT, and compares them to a narrow band model without any carrier trapping, i.e., the straight lines in Fig. 2D [2]. Overall, Fig. 2 summarizes 3 universal observations in the nondegenerate regime: (a) The Seebeck coefficient in organic polymers are large, i.e., much larger than $k_B/e \approx 86$ μV/K (e, elementary charge); (b) they are decreasing functions of increasing carrier concentration n; and (c) they are independent of temperature (within the measurement error) between the measurable range of 200 and 300 K. Temperature-independent Seebeck coefficients over a similar temperature range were also reported for single crystals of the molecular semiconductors pentacene and rubrene [41].

There were attempts to interpret the Seebeck coefficient and field effect transistor measurements as functions of temperature consistently in terms of disorder-induced variable range hopping (VRH) akin to models used to explain similar measurements in amorphous silicon [42,43]. For PBTTT and PSeDPPBT, this might be possible, but the fits depend on several unknown and unmeasurable parameters [36]. In addition, such VRH models break down for IDTBT [2]. A simpler, more consistent interpretation of the 3 salient Seebeck features, applicable to all polymers in the nondegenerate transport regime, is given by a narrow-band model in which charge carriers experience a small degree of energetic disorder and can access a temperature-independent density of thermally accessible sites. The narrowness of the carriers' energy bands is probably due to polaron formation [12], an assumption that is supported by charge accumulation spectroscopy [2]. In the simplest narrow-band model, the Seebeck coefficient is expressed as [12]

$$\alpha = \frac{k_B}{e}\ln\left(\frac{N-n}{n}\right) + \frac{k_B}{e}\ln(2) + \alpha_{vib}.$$

It is the sum of 3 contributions. The first contribution is the change of the entropy of mixing when the density of mobile polarons is n and the density of thermally accessible sites is N. The second contribution is the entropy change arising from the 2-fold spin degeneracy. The final term is the high-temperature limit of the entropy change produced by a polaron altering the stiffness or frequencies of the molecular vibrations. Only the first contribution depends explicitly on carrier density. A plot of α versus the logarithm of the mobile carrier density n yields a straight line with slope $-\frac{k_B}{e} \times \ln(10) = -198\ \mu V\ K^{-1}\ decade^{-1}$.

From Fig. 2, the slopes of the linear experimental α–log(n) plots depend on the specific polymer and exceed $-198\ \mu V\ K^{-1}$ $decade^{-1}$. These discrepancies are reconciled by accounting for a fraction f of the n injected carriers, which are trapped in shallow traps and do not participate in entropy transport. In this case, n is replaced by $n(1-f)$ and the slope of the α–log(n) plot is increased to $-\frac{k_B}{e} \times \ln(10)/(1-f)$. This procedure is justified when the band-tail-like traps are within $\sim k_B T$ of the narrow band of conducting polaron states. One can extract values of f equal to 0.3, 0.5, and 0.7 for IDTBT, PBTTT, and PSeDPPBT, respectively. This procedure demonstrates that there is much less trapping in IDTBT compared to PBTTT or PSeDPPBT. Using such gate voltage-modulated Seebeck coefficient measurements, IDTBT was shown to have most of its charge carriers residing in mobile states. It is now also known that the slope of the Seebeck coefficient on α–log(n) depends sensitively on the properties of the polymer at the time of measurement. Since organic polymers can dynamically alter their properties depending on ambient influences, α–log(n) plots have also been used to map asymptotic stability [44].

To interpret the magnitude of the Seebeck coefficients, we estimated the number of equivalent sites in the polymers. By assuming that there is one equivalent site on each polymer repeat unit (consistent with small polarons), we obtain $N = 7.4 \times 10^{20}\ cm^{-3}$ (IDTBT) and $N = 8.9 \times 10^{20}\ cm^{-3}$ (PBTTT), based on reported unit cell parameters [45,46]. The solid black and red lines in Fig. 2D are the resulting estimates of the Seebeck coefficients for IDTBT and PBTTT, respectively, on ignoring any carrier-induced changes in these molecules' vibrations. The small discrepancies between the solid lines of Fig. 2D and the experimental data in Fig. 2D may be assumed to indicate a vibrational contribution, but in fact, the difference was later shown to be an artifact of how the magnitude of the Seebeck

coefficient was extracted using the resistance thermometer's estimate of the temperature difference. With a more accurate estimate of the on-chip temperature difference, the Seebeck coefficients of organic polymers were found to show a negligible vibrational contribution [3,44,47]. Organic small molecules, on the other hand, may have a more substantial contribution to the Seebeck coefficient from vibrational entropy. For example, pentacene was shown to have a vibrational contribution of 265 μV/K [48]. Preliminary studies on C_8-BTBT and C_{10}-DNTT were shown to have a smaller contribution, potentially less than 100 μV/K [49]. In comparison, inorganic materials such as boron carbides have a vibrational contribution to the Seebeck coefficient of 200 μV K^{-1} at 300 K [50]. Whether the Seebeck coefficient is an appropriate technique to estimate the vibrational entropy of organic molecular semiconductors requires broader experimental investigation to arrive at a conclusive answer.

Lastly, the temperature invariance of the Seebeck coefficient in the nondegenerate regime is a direct consequence of its expression in terms of the entropy of mixing, spin degeneracy, and its vibrational contribution. The lack of temperature dependence in this equation is due to polaronic bands being narrow and on the order of k_BT, causing all the states for transport to remain available at all temperatures.

As the carrier concentration in the organic semiconductor is increased, it goes from the nondegenerate regime ($n \ll N$) to the near-degenerate regime $n \approx N$. In the near-degenerate regime, the properties of the Seebeck coefficient, the electrical conductivity, and their interrelationship are significantly different from those discussed above and constitute the content of the next section.

Thermoelectric Transport in Organic Polymers within the Near-Degenerate Regime of Transport

The semicrystalline semiconducting polymer PBTTT has been studied intensively for its ability to achieve large electrical conductivities reported to cross 1000 S/cm upon doping [1,51]. Enhanced conductivities such as these are not a consequence of increased mobility. They are due to an increase in carrier density. This fact is now known based on Hall effect measurements, which show that the carrier mobility remains constant as the dopant-induced carrier density increases [52,53]. Thus, large electrical conductivities bring the organic semiconductor within the realm of the near-degenerate transport regime where $n \approx N$.

Figure 3 shows the relationship between the Seebeck coefficient and the electrical conductivity within the near-degenerate transport regime in PBTTT. In this highly doped regime, it is customary to plot the Seebeck coefficient against the conductivity, rather than against the carrier density. The reason for this is 3-fold. (a) The side-gate geometry of the electrolyte-gated devices has liquid- or gel-based dielectrics whose exact dimensions are not always known, (b) the dopants can infuse into the bulk of the organic semiconductor upon gating, and (c) the ease in performing 4-point probe electrical measurements when the electrical conductivities are substantial.

It is clear from Fig. 3A, which includes several data points of PBTTT doped with various doping techniques, that the Seebeck coefficient varies with conductivity in a seemingly counterintuitive fashion. In the low conductivity regime on this log–log plot, the Seebeck reduces linearly and gradually as the conductivity increases. At large conductivities, greater than 100 S/cm on this plot, the Seebeck coefficient reduces drastically upon increasing the conductivity. In terms of empirical scaling laws, the Seebeck–conductivity relationship goes from showing an $S \propto \sigma^{-1/4}$ dependence in the low conductivity regime to an $S \propto \sigma^{-1}$ dependence in the high conductivity regime. Figure 3B shows another plot of the Seebeck–conductivity relationship in PBTTT from different work [54]. The outcome of both experiments is equivalent in that they increase the conductivity from the nondegenerate regime to the near-degenerate regime. In Fig. 3B, a piecewise subdivision in the Seebeck–conductivity plot was suggested using 3 empirical scaling laws, namely, $S \propto \sigma^{-1/4}$ in the low conductivity regime suggestive of VRH, $S \propto \sigma^{-1/3}$ in an intermediate conductivity regime suggestive of weak localization, and $S \propto \sigma^{-1}$ in the high conductivity regime suggestive of so-called metallic transport [55]. Carrier density modulation of temperature-dependent conductivity as well as magnetoconductance on this ion gel-gated sample of PBTTT were also carried out to appropriate the various transport regimes shown on Fig. 3B [54]. Figure 3C shows the behavior of the Seebeck coefficient and power factor of ionic liquid gated PBTTT [56]. The inset shows a linear–log plot of the Seebeck coefficient versus conductivity, where the dotted line represents a slope of -198 μV/K per decade. Clearly, the experimentally measured slope in the highly doped regime is much shallower than this nondegenerate value. Across the same region of the transition where the Seebeck coefficient begins to plummet upon increasing the conductivity, the power factor registers a maxima. There is an observed scaling law in the power factor versus conductivity in the nondegenerate limit of low conductivity, i.e., $S^2\sigma \propto \sigma^{+1/2}$. This is a direct consequence of the power factor being $S^2\sigma$ and of $S \propto \sigma^{-1/4}$ in the same regime. There is no evident scaling law for the power factor in the so-called metallic regime where $S \propto \sigma^{-1}$. Figure 3D shows the Seebeck coefficient versus conductivity and the power factor versus conductivity of various ion gel-gated DPP-based polymers [57]. Once again, it is clear from this plot that upon achieving large conductivities, the Seebeck coefficient undergoes a rapid reduction. The power factor exhibits a maxima in these DPP-based polymers around the same conductivity at which a transition in trend was seen. It is also clear that the different DPP-based polymers have slightly different trends, with PDPP4T having the steepest drop in the Seebeck coefficient and in the power factor within the measurable range. At very large near-degenerate carrier densities, it is less probable that a large fraction of the induced carrier density is caught up in trap states as argued in the nondegenerate regime. The differences between the DPPs on the $S - \sigma$ plot may thus suggest intrinsic differences in the maximum possible conductivity achievable in these systems as discussed later in this review article [35].

It has been suggested that such trend transitions in the conductivity upon increasing the carrier density are akin to an insulator-to-metal transition where carriers go from being localized to being delocalized [6,7,56]. From a thermodynamic viewpoint, however, a metal-insulator transition is a first-order phase transition. In such a transition, the structure and properties are expected to change abruptly. In addition, in first-order phase transitions (such as ice to water), there is a latent heat associated with the transition and a discontinuity in derivative properties such as the heat capacity. Such findings are yet to be reported for highly doped organic semiconductors to unambiguously confirm the hypothesis linked to the insulator-to-metal transition. There are indeed structural changes, such as a swelling of the organic semiconductor to accommodate dopants when doping to high

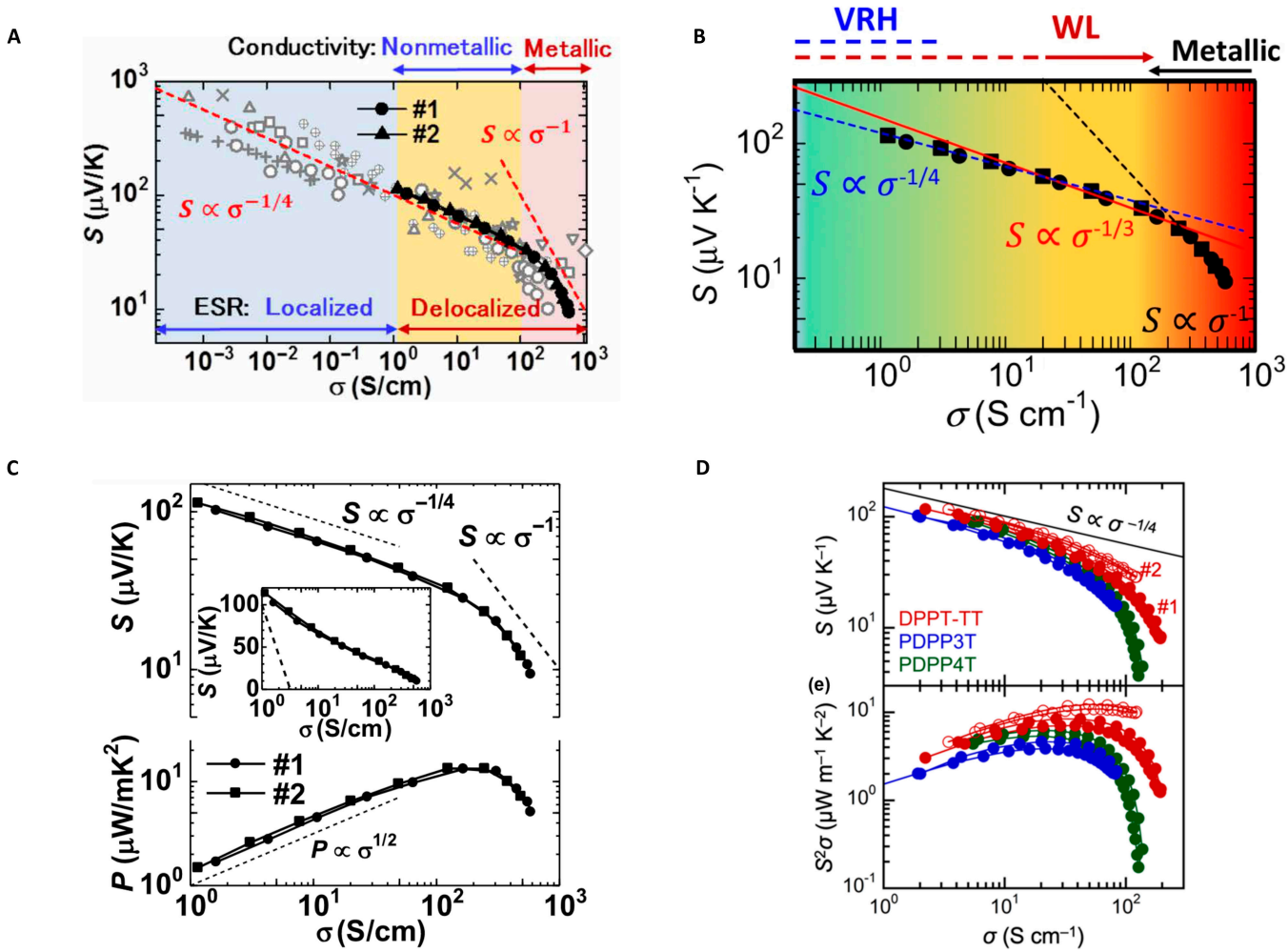

Fig. 3. Seebeck coefficient in organic polymers within the near-degenerate regime of transport. (A) Seebeck–conductivity ($S - \sigma$) plots in PBTTT over a broad range of conductivities achieved using different methods of doping [56]. (B) Electrical conductivity dependence of the Seebeck coefficient in PBTTT obtained with electrolyte gating at room temperature [54]. (C) Both Seebeck and power factor dependence on electrical conductivity obtained with electrolyte gating. This figure corresponds to the data shown in (A) and is taken from the same publication. (D) Electrical conductivity dependence of the Seebeck coefficient and the thermoelectric power factor obtained with electrolyte gating in various DPP-based polymers [57]. In all the plots, piecewise smooth empirical scaling laws between σ and S have been indicated. Image taken from [54,56,57].

carrier densities, but these changes are gradual [8,56]. Lastly, it is known that electrochemical doping can also enhance structural order within a polymer film upon dopant molecule uptake, and not always introduce structural distortion [58]. Such electrochemical doping-enhanced structural order was seen in the polymer poly[bis(3-dodecyl-2-thienyl)-2,2-dithiophene-5,5-diyl] (PQT) with low side chain density [58]. Irrespective of this enhancement of order, similar $S - \sigma$ trends were seen in PQT as were seen in PBTTT and in the DPPs shown in Fig. 3. This suggests that both inducing structure upon doping (as in PQT) and/or distorting structure upon doping (as in PBTTT) lead to similar trends in $S - \sigma$ behavior at large carrier densities. It is hence likely that the observed $S - \sigma$ trends in the near-degenerate regime are a consequence of a more fundamental and universal carrier transport property of organic semiconductors.

It ought to be explicitly mentioned here that despite being overused in the literature, the observed scaling laws of $S \propto \sigma^{-1/4}$ and $S^2\sigma \propto \sigma^{+1/2}$ in the low conductivity regime are purely empirical [59]. As of this writing, there is still no documented physical underpinning for why these laws arise, besides being founded on some form of VRH transport. In the same spirit, $S \propto \sigma^{-1}$ in the high conductivity regime is only an observation where a correlation is made based on what metallic transport is known to look like.

Another pertinent and closely related observation in the near-degenerate transport regime is the temperature dependence of the conductivity and the Seebeck coefficient of highly doped organic polymers. Shown in Fig. 4 is the temperature dependence of PBTTT films doped using 3 different techniques of varying doping efficiency [60]. It is interesting to note here that although the conductivity is thermally activated, the Seebeck coefficient displays a linear dependence on temperature. This behavior in the highly doped near-degenerate regime contrasts the temperature invariance seen in the Seebeck coefficient within the nondegenerate regime. The linear dependence in temperature on the $S - T$ plot has caused intense speculation on whether highly doped polymers sport metallic transport governed by the Mott formula under the rigid band approximation, namely, $S = -\frac{\pi^2 {k_B}^2 T}{3e}\left[\frac{d \ln \sigma_E}{dE}\right]_{E=E_F}$ [60]. The fact that the measured conductivity is indicative of hopping transport, but the Seebeck coefficient is assumed to be metallic,

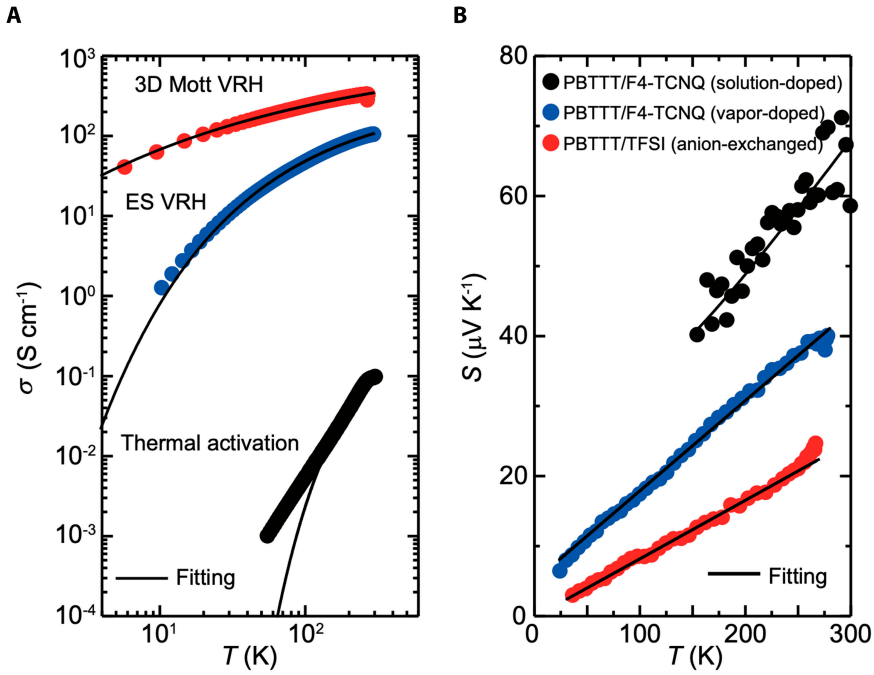

Fig. 4. Temperature dependence of the electrical conductivity and the Seebeck coefficient in doped PBTTT. (A) Temperature-dependent conductivity in PBTTT depending on the nature of doping. The doping efficiency, and thus the active carrier density, is largest for anion-exchanged doping and lowest for solution doping. (B) Corresponding Seebeck coefficient as a function of temperature in doped PBTTT for different doping levels. Image taken from [60].

represents a clear dissonance in the literature. Although an explanation was attempted for these tandem observations in the semicrystalline polymer PBTTT, and said to indicate metallic conduction within ordered domains [60], a more convincing explanation may be built based on polaronic transport in organic semiconductors. We build arguments for such a case later in this work.

All told, the salient features of thermoelectric transport in highly doped organic semiconductors within, or close to, the near-degenerate regime are as follows. First, the Seebeck coefficient in highly doped organic polymers is small, i.e., smaller than $k_B/e \approx 86$ μV/K. Second, the Seebeck coefficient varies linearly with conductivity on a log–log plot for nondegenerate conductivities but shows a sudden drop at near-degenerate conductivities. The curve remains continuous and differentiable at the transition. Third, empirical scaling relationships between S and σ seem to fit only small segments of the full $S-\sigma$ curve, but a universal fit over the whole carrier density range is not possible. Fourth, the power factor registers a maxima at very large near-degenerate carrier densities. Fifth, the slope of the $S-\log(\sigma)$ is much shallower than its nondegenerate value of −198 μV/K per decade. Sixth, the electrical conductivity shows a hopping-like behavior as a function of temperature, but the Seebeck coefficient shows a metallic-like behavior with a direct proportionality to temperature.

The above 6-fold observations of thermoelectric transport in highly doped organic semiconductors may be explained based on a narrow band polaron model as described in the next section.

Jonker-Type Analysis for Polaronic Transport in Organic Semiconductors

In this section, we demonstrate how the empirical trends of $S \propto \sigma^{-1/4}$ and $S^2\sigma \propto \sigma^{1/2}$ may fundamentally be a consequence of polaronic charge carrier hopping in the organic semiconductor within the nondegenerate regime of carrier densities, 10^{19} cm^{-3} or fewer, and within the applicability of Boltzmann statistics [2–4]. We also show how the $S-\sigma$ relationship, interpreted within the dictates of polaronic hopping, explains the origin of the 6-fold observations of the near-degenerate transport regime.

The characteristic features of small polaron conduction can be seen through equations for their electrical conductivity and Seebeck coefficient. The electrical conductivity is given by the Nernst–Einstein equation, $\sigma = (Nc)e\mu = \frac{(Nc)eD}{k_BT}$, where N is the total density of available hopping sites, with c being its fractional occupancy. μ is the carrier mobility, T is the temperature, e is the electronic charge, k_B is the Boltzmann constant, and D is the small polaron diffusivity, $D = g(1-c)ea^2\nu\exp\left(-\frac{E_H}{k_BT}\right)$ [35]. In the equation for the small polaron diffusivity, g is a geometric factor, a is the jump distance between equivalent hopping sites, ν is the lattice vibrational frequency, and E_H is the hopping energy. The polaron conductivity is thus written as $\sigma = \frac{gNc(1-c)\ e^2a^2\ \nu}{k_BT}\exp\left(-\frac{E_H}{k_BT}\right)$. The small polaron Seebeck coefficient on the other hand is $S = \pm\frac{k_B}{e}\ln\left[\frac{2(1-c)}{c}\right]$, where the parameters hold their usual meanings [61–63]. The sign ± indicates the polarity of the small polaron, either hole or electron. The polarity of the Seebeck coefficient can invert depending on the fractional occupancy, c, here [64].

A characteristic of small polaron hopping is the $\frac{1}{T}$ dependence in the prefactor of the conductivity. One way to validate this temperature dependence in the prefactor is to fix the carrier density in the system and measure the conductivity as a function of temperature over a broad range. In the presence of smaller hopping energies that come into effect at high carrier

densities, there is a tendency for the exponential term in the equation for the conductivity to cancel out the k_BT term in the denominator of its prefactor. This implies that the conductivity tends to show an even weaker thermally activated behavior from its original $\exp\left(-\frac{E_H}{k_BT}\right)$ dependence. Such a transition in trend has indeed already been observed in the doped polymer PBTTT, reproduced in Fig. 4, where its solution-doped (low doping efficiency) avatar is strongly "thermally activated", while its anion exchange-doped (high doping efficiency) avatar shows a much weaker temperature dependence in the conductivity [60].

Several decades ago, Jonker [65] developed quantitative relationships between transport parameters in semiconductors of either p-type, n-type, or mixed conduction by plotting "pear-shaped" curves between the Seebeck coefficient and the conductivity. Several insights into the conduction parameters can be obtained using "Jonker-pears", such as the DOS-mobility product and the intrinsic bandgap of the semiconductor. Jonker mentions in his work that the analysis is applicable to nondegenerate semiconductors where Boltzmann statistics can be applied. He unequivocally states in his paper that an uncertainty in the construction of $S - \log(\sigma)$ can arise for higher doping concentrations. For this reason, in his original paper, Jonker generates the plot of $S - \log(\sigma)$ in PbS with carrier densities that go up to only 10^{19} cm^{-3} [65]. Jonker's well-known model proposed the existence of a slope having a value $-\frac{k_B}{e}$ or −86.15 μV/K on a plot of $S - \ln(\sigma)$. This can also be written as $-\frac{k_B}{e}\ln(10)$, which is −198 μV/K per decade on a plot of $S - \log(\sigma)$ [65]. The same value of slope arises on a plot of $S - \ln(n)$ when assuming transport in narrow bands and where the Seebeck coefficient takes the form of the temperature invariant Heikes formula, $S \approx \frac{k_B}{e}\ln\left(\frac{N}{n}\right)$ [2,13,34,55,66–68]. Heikes formula is based on the entropic argument that considers the number of ways the carrier density n can be statistically distributed over N available states. It is another way to justify why the observed slope on an $S - \log(n)$ plot is equal to $-\frac{k_B}{e}\ln(10)$ in the absence of trap states [67].

The original analysis of the Seebeck coefficient and the electrical conductivity in the nondegenerate regime was developed by Jonker in 1968 [65] and later modified by Nell and coworkers in 1989 [35] to account for observed transport trends in the near-degenerate regime within conductive oxides. When the carrier density in organic semiconductors crosses the 10^{20} cm^{-3} threshold, a condition achieved in ionic gel-gated organic devices, carrier transport enters the near-degenerate regime as discussed earlier [54,56–58]. Within this near-degenerate regime, Boltzmann statistics does not hold and corrections to the Seebeck coefficient and the conductivity from their nondegenerate behavior need to be accounted for. Such corrections lead to a maximum in the power factor irrespective of chemical composition of the organic semiconductor as shown in this work.

By defining the ratio $q = c/(1-c)$, one can use the previous expression for the polaronic Seebeck coefficient, namely, $S = \pm\frac{k_B}{e}\ln\left[\frac{2(1-c)}{c}\right]$, to write $q = \frac{c}{1-c} = 2\exp\left(+Se/k_B\right)$ for an n-type polaronic system or $q = \frac{c}{1-c} = 2\exp\left(-Se/k_B\right)$ for a p-type polaronic system. The product $c(1-c)$ can thus be written as,

$$c(1-c) = \frac{q}{\left(1+q\right)^2}.$$

The same product appears in the expression for the polaronic conductivity above, namely, $c(1-c) = \frac{\sigma}{\Omega N\nu}\exp\left(\frac{E_H}{k_BT}\right)$, with $\Omega = \frac{ge^2a^2}{k_BT}$. Under a bold assumption on the conductivity (which will be corrected for later in this article), namely, that the hopping energy E_H, the lattice vibrational frequency ν, and the number of available states N do not change upon doping, the maximum conductivity σ_{max} will occur at $c = 0.5$. Normalizing the conductivity thus leads to the following equation:

$$\frac{c(1-c)}{0.5^2} = \frac{\sigma}{\sigma_{max}}.$$

On grouping the equations relating to $c(1-c)$, we arrive at a transcendental equation that links the Seebeck coefficient with the conductivity, namely,

$$\frac{1}{0.5^2}\frac{q}{\left(1+q\right)^2} = \frac{\sigma}{\sigma_{max}}.$$

In the case of a p-type polaronic system, this can explicitly be written in terms of S and σ as,

$$\frac{1}{0.5^2}\frac{2\exp\left(-\frac{Se}{k_B}\right)}{\left[1+2\exp\left(-\frac{Se}{k_B}\right)\right]^2} = \frac{\sigma}{\sigma_{max}}.$$

For an n-type polaronic system, the transcendental equation reads

$$\frac{1}{0.5^2}\frac{2\exp\left(+\frac{Se}{k_B}\right)}{\left[1+2\exp\left(+\frac{Se}{k_B}\right)\right]^2} = \frac{\sigma}{\sigma_{max}}.$$

Similar $S - \sigma$ relationships can be derived for spinless bipolarons, should it be the case that bipolaron formation dictates transport in doped organic semiconductors at large carrier densities [69].

A plot of both p-type and n-type relationships between the Seebeck coefficient and the electrical conductivity dictated by these equations are shown in Fig. 5A. Figure 5A also plots the Jonker slope for a semiconductor as a dotted line. Salient features of small polaron conduction as predicted by the model of Fig. 5A are as follows. First, at large conductivities close to the near-degenerate regime, the Seebeck coefficient is small, i.e., much smaller than $k_B/e \approx 86$ μV/K. Second, in the regime of low electrical conductivity, the Jonker model (whether for band type or for small polarons) has a very similar slope to that of the small polaron model. In the regime of large conductivities, however, the 2 models diverge. This is because the assumptions of the Jonker model no longer hold close to the highest conductivities in polaronic conductors. Third, the Seebeck coefficient decreases gradually on the linear–log plot of $S - \sigma$ at low conductivities. At larger conductivities, close to the maximum supported by the polaronic conductor, the Seebeck coefficient drastically reduces. Fourth, the Seebeck coefficient can invert in sign at carrier densities beyond the maximum carrier density. In other words, it can show a negative (positive) polarity, although polarons may be p-type (n-type).

Figure 5B plots only the p-type component of the small polaron Seebeck coefficient in the regime of positive Seebeck coefficients on a log–log plot. This log–log plot visualization is

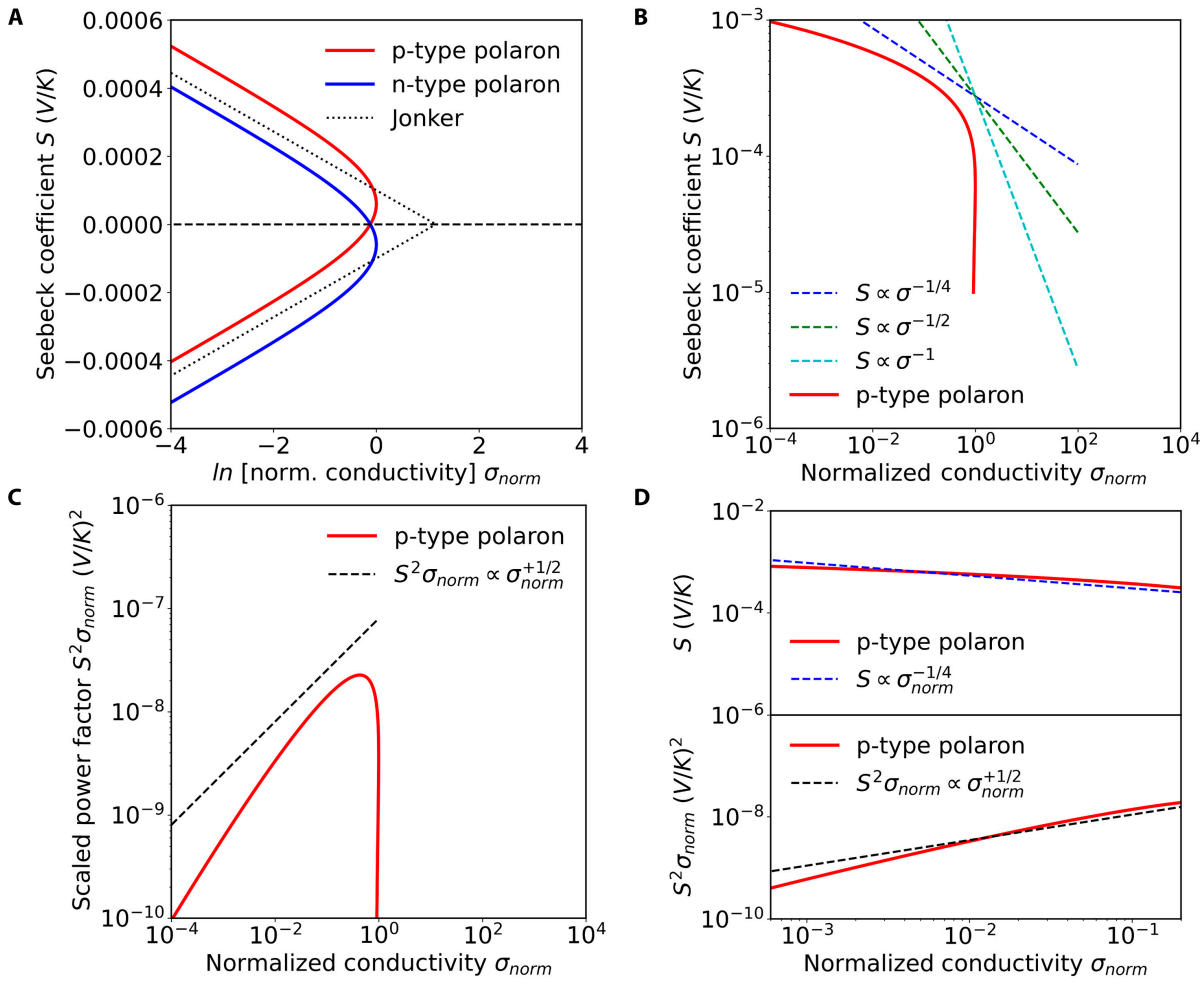

Fig. 5. Jonker-type analysis for small polaron conduction. (A) $S-\sigma$ relationships for p-type and n-type polarons compared with the conventional Jonker slope on a linear–log plot. (B) p-type polaron behavior on a log–log plot of $S-\sigma$ compared with empirical trends used in the literature, namely, $S \propto \sigma^{-1/4}$, $S \propto \sigma^{-1/2}$, and $S \propto \sigma^{-1}$. (C) Log–log plot of power factor versus normalized conductivity of p-type polarons showing a maxima in the power factor. A comparison is also made with the empirical trend $S^2\sigma \propto \sigma^{+1/2}$. (D) Comparisons of the p-type polaron model with empirical relationships used in literature for the nondegenerate transport regime.

done because most published works have plotted $S-\sigma$ relationships on a log–log plot [56,57,59,70–73]. Figure 5B also shows dotted lines of 3 empirical trends, namely, $S \propto \sigma^{-1/4}$, $S \propto \sigma^{-1/2}$, and $S \propto \sigma^{-1}$. None of these empirical trends fit the transition, but they go to show that their gradual change from one to the other does envelope the continuous polaron function. Such a transition in empirical trend was used to justify the possible presence of an insulator to metal transition between a hopping regime of transport and a metallic regime of transport. The $S-\sigma$ plot constructed in Fig. 5B for polarons is both continuous and differentiable and so may not represent an unambiguous first-order phase transition.

From Fig. 5B, the magnitude of the Seebeck coefficient in highly doped organic devices within the near-degenerate regime is also smaller (about tens of μV/K) than those in the nondegenerate regime (about hundreds of μV/K). That said, it is still larger than the magnitude of the Seebeck coefficient in a conventional metal with a well-defined Fermi sea (less than tens of μV/K).

Figure 5C uses the $S-\sigma$ predictions of the polaron model shown in Fig. 5B to construct the power factor of the system. The conductivity used here is the normalized conductivity of the polaronic system $\frac{\sigma}{\sigma_{\max}}$, which is why the units have been changed appropriately. It is evident from Fig. 5C that the model clearly predicts a maximum in the power factor for polaronic conduction. Figure 5C also plots the empirical scaling behavior $S^2\sigma \propto \sigma^{1/2}$, showing an agreement between the model and the empirical trend over the region of normalized conductivity close to the maxima.

Figure 5D plots both the polaronic model for the Seebeck coefficient and the power factor together with the empirical scaling trends, $S \propto \sigma^{-\frac{1}{4}}$ and $S^2\sigma \propto \sigma^{\frac{1}{2}}$, but only over 2 orders of magnitude, as this is the range measured in prior experiments shown in Fig. 3. It is evident that the polaronic model resembles the empirical scaling trends over these 2 orders of magnitude. One can argue that the agreement would be improved if a randomized scatter resembling experiment is superposed over the polaron model prediction.

So far, Fig. 5 can simulate 4 of the 6-fold observations of the experiments in the near-degenerate regime. First, it dictates that the Seebeck coefficients in the near-degenerate regime are small. Second, it predicts both the original Jonker slope in the regime of low conductivities (nondegenerate regime) and the sudden drop in the Seebeck coefficient at large conductivities (near-degenerate regime). Third, the continuous trend in $S-\sigma$

supports the piecewise empirical relationships used in the literature (Fig. 3) between S and σ, namely, $S \propto \sigma^{-1/4}$ and $S \propto \sigma^{-1}$. Fourth, it predicts a maximum in the power factor at near-degenerate carrier densities.

To predict the fifth observation, namely, reduced slopes $\frac{\partial S}{\partial \log(n)} < -\frac{k_B}{e}\ln(10)$ on the $S - \log(\sigma)$ plot of Fig. 3 in the high conductivity regime, one needs to understand the shortcoming of the polaron model and apply justifiable corrections. In deriving the $S - \sigma_{norm}$ used in Fig. 5, it was assumed that the maximum conductivity, σ_{max}, that was used to scale the total conductivity σ in the polaronic system had the same total number of available hopping sites N, the same frequency ν, and the same hopping energy E_H. The frequency ν and the hopping energy E_H need not be constant upon doping the system to increase its electrical conductivity. Both the electrical conductivity and the Seebeck coefficient in the system are transport parameters reliant on the hopping parameters. As the doping in the system is increased, it is expected that the hopping rate will also increase. An increased hopping rate will increase the maximum conductivity of the system but is expected to simultaneously reduce the Seebeck coefficient from its ideal value shown in Fig. 5. This is intuitively understood based on how the Seebeck coefficient is linked with the electrical conductivity in the most general case [74]. To incorporate the above rationale, we introduce a corrective dimensionless scaling factor γ to reduce the Seebeck coefficient upon doping. Within the literature, such a single-parameter scaling of the Seebeck coefficient was done to explain $S - \sigma$ relationships in carbon nanotubes [75]. Another potent article that incorporates the scaling factor for organic polymers specifically is by Mateeva et al. [76]. In their work, the scaling factor is refered to as a "pure number". The pure number, when equal to 1, represents a polymer system with the maximum possible ZT. Our γ parameter analysis is also similar to the single-parameter electronic quality factor developed to understand and compare the power factors in inorganic thermoelectrics [77]. A scaling factor greater than 1 is an indication that the system cannot be characterized exactly by the transport equations for polarons shown earlier, and that the assumption on the conductivity made, namely, that the hopping energy E_H, the phonon frequency ν, and the number of available states N do not change upon doping, must be called into question. A scaling factor greater than 1 could also indicate a departure from the adiabatic case for polaron motion, since the equations for conductivity used in our analysis are for adiabatic hopping of polarons.

Intuitively, when considering a reduction in the hopping energy E_H upon doping, we assume that the Seebeck coefficient would reduce to S/γ, where γ goes from 1 to approximately 10 in organic semiconductors. On a log–log plot, the scaling factor γ preserves the sudden drop in Seebeck at the absolute maximum permissible conductivities. Figure 6 shows the effect of this intuitive dimensionless factor γ on the relationship between the Seebeck coefficient and the electrical conductivity. Figure 6A shows, on a log–log plot, how the Seebeck coefficient reduces upon increasing γ from 1 to 9.

To understand how such an analysis affects the slopes of the Seebeck coefficient on an $S - \log(\sigma)$ plot and predict $\frac{\partial S}{\partial \log(n)} < -\frac{k_B}{e}\ln(10)$, Fig. 6B plots the contents of Fig. 6A on a linear–log plot. It is evident from this plot that an increasing value of γ gives rise to a reduced slope. Although plotted for normalized conductivities down to 10^{-4}, it should be emphasized that these reduced slopes will affect only the near-degenerate regime of conductivities in actual experiments.

Such slopes on an $S - \log(n)$ plot, smaller than $-\frac{k_B}{e}\ln(10)$ in magnitude, have indeed been observed in measurements on ion gel electrolyte-gated Seebeck measurements on organic semiconductors [56,57]. Slopes smaller than $-\frac{k_B}{e}\ln(10)$ in magnitude on a plot of $S -$ log (n) have also been observed in material systems such as carbon nanotube-based composites. In single-walled carbon nanotube networks, for example, the onset of the deviation from $\frac{\partial S}{\partial \log(n)} = -\frac{k_B}{e}\ln(10)$ to $\frac{\partial S}{\partial \log(n)} < -\frac{k_B}{e}\ln(10)$ is seen at carrier densities greater than 10^{19} cm^{-3} [78].

One way to understand why the slopes on an $S - \log(n)$ plot can be lower than $-\frac{k_B}{e}\ln(10)$ in magnitude within the near-degenerate regime is to understand that in the near-degenerate regime of measurement, the implicit assumptions of the Jonker analysis break down. At these large carrier densities, configurational entropy may not primarily govern the Seebeck coefficient any longer, and Heikes formula may be violated. The reduced carrier concentration dependence of the Seebeck coefficient may be due to this manifestation of Boltzmann statistics becoming insufficient possibly due to the Fermi level (E_F) approaching the state distribution (i.e., $n \ll N$ does not hold). In such a regime, the narrow-band description for which Heikes formula is applicable becomes inappropriate, and it is speculated that the actual DOS of the networks needs to be considered [78].

Another class of materials in which $\frac{\partial S}{\partial \log(n)} < -\frac{k_B}{e}\ln(10)$ has been observed is the multifunctional conductive oxides [79,80]. Amorphous conductive oxides and organic semiconductors have much in common from a transport point of view, seeing as disorder can be a governing factor for the electronic transport behavior they demonstrate. In amorphous InGaZnO, for example, the slopes on the $S - \log(\sigma)$ plot are between −54 μV/K and −70 μV/K per decade, i.e., much smaller than the expected ideal slope of −198 μV/K per decade. This behavior was ascribed to the hydrogenation of InGaZnO, which rendered its conduction metallic. A related example where the ideal slope of $S - \log(\sigma)$ deviated from that predicted by the Jonker analysis is in Al-doped ZnO [81]. Further examples of the same deviation were seen in several oxide-based systems from spinel ferrites and nonstoichiometric oxides to highly doped systems such as $LaCrO_3$:Sr and Mn_3O_4:Fe [35]. In the latter, a Jonker-like analysis was used to distinguish small polaron hopping from band-type semiconductivity. This work included a balanced discussion of the strengths and limitations of Jonker's analysis [65].

All told, within our intuitive assumption of scaling the Seebeck coefficient by a dimensionless quantity γ in highly doped organic semiconductors, reduced slopes $\frac{\partial S}{\partial \log(n)} < -\frac{k_B}{e}\ln(10)$ are predicted.

To use the scaled model of Fig. 6 to fit experimental plots of $S - \sigma$, one will need to multiply the normalized conductivity σ_{norm} with the maximum conductivity σ_{max} obtained from the experiment. This will shift the conductivity appropriately along the x axis. Along the y axis, the Seebeck coefficient of the model is shifted down by dividing the Seebeck coefficient by γ to meet the experimental curve. Figure 6C shows an $S - \sigma$ dataset of doped polymer PDPP4T published in the supplementary

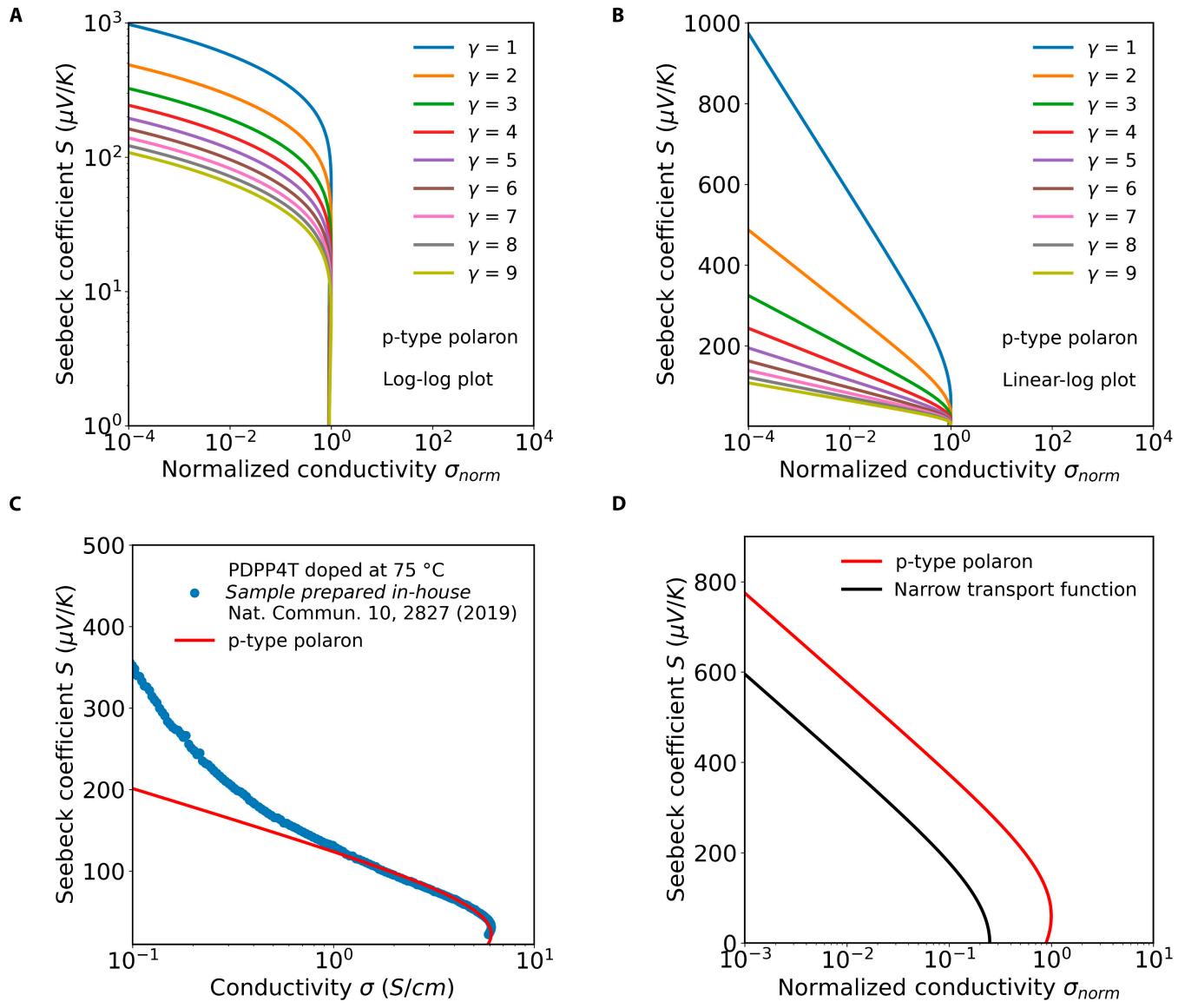

Fig. 6. $S-\sigma$ plots scaled by a dimensionless factor γ. (A) $S/\gamma-\sigma$ relationships for p-type polarons on a log–log plot. (B) $S/\gamma-\sigma$ relationships for p-type polarons on a linear–log plot. (C) Scaled $S-\sigma$ plot fit to data from [70], showing the point of maximum in the conductivity both in the experimental data and in the model. (D) Comparison between the p-type polaron model and the narrow transport function for a given normalized conductivity. In the case of the p-type polaron model, $\sigma_{\text{norm}} = \frac{\sigma}{\sigma_{\text{max}}}$. In the case of the narrow transport function, $\sigma_{\text{norm}} = \frac{\sigma}{\sigma_{E_0}}$.

materials of [70]. Clearly, the data show a maximum in the conductivity, σ_{max}, after which there is a reversal in trend. Our scaled polaron model can be fit to the high conductivity regime of the measurement with a $\gamma = 2.65$. The maximum conductivity in this system is around 6 S/cm. At even lower conductivity on this plot, there is a deviation in trend from the polaronic model most probably because of the operation of a different hopping mechanism [82].

Figure 6D shows a comparison of the unscaled or ideal ($\gamma = 1$) polaron model with a narrow band transport function that has been used in the past to describe similar $S-\sigma$ trends within oxides where conduction occurs in narrow bands [83]. The narrow band transport function plotted here is described by [83]

$$\frac{\sigma}{\sigma_{E_0}}\left[1+\exp\left(+\frac{Se}{k_B}\right)\right]\left[1+\exp\left(-\frac{Se}{k_B}\right)\right]=1.$$

The normalized conductivity of this narrow transport function plotted in Fig. 6D is $\sigma_{\text{norm}} = \frac{\sigma}{\sigma_{E_0}}$ where σ_{E0} is the scaling factor. The polaron model we deploy has much in common with this narrow transport function. While the trends are similar, the polaron model clearly shows a maximum σ_{max} in the conductivity within the positive range of the Seebeck coefficient after which there is a reversal in trend. Since such behavior has been observed in doped organic semiconductors, such as shown in Fig. 6C, the function that describes polaronic transport is probably more appropriate to use when analyzing most organic semiconductors. The polymer IDTBT may behave differently when doped to high carrier densities. On account of its narrow bands, it may be better described with the narrow transport function shown in Fig 6D where the maxima in conductivity occurs when the Seebeck coefficient is 0 μV/K.

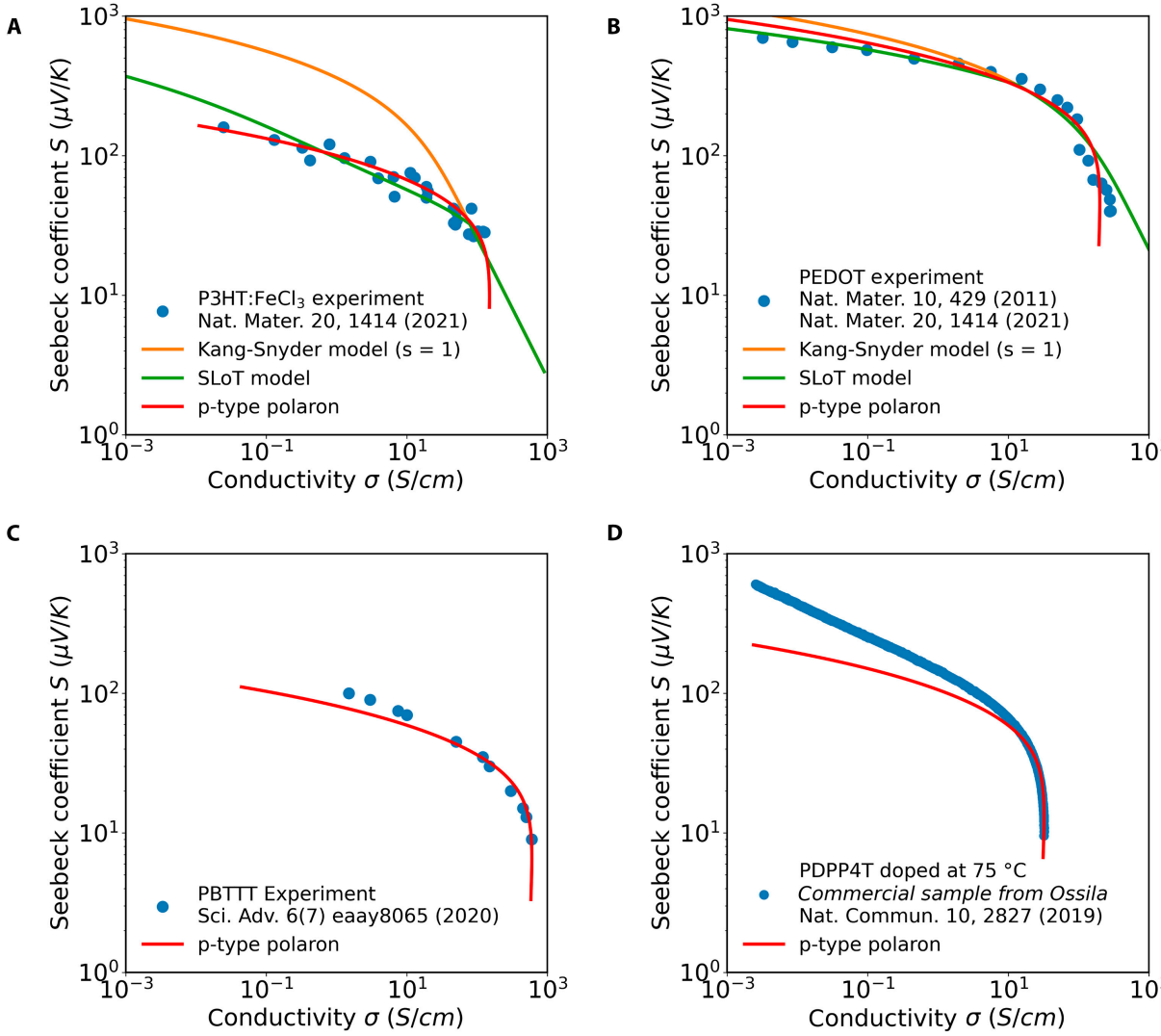

Fig. 7. Polaron model fit to $S-\sigma$ experimental observations. (A) $S-\sigma$ fit to P3HT data in [85]. (B) $S-\sigma$ fit to PEDOT data in [101]. (C) $S-\sigma$ fit to PBTTT data in [56]. (D) $S-\sigma$ fit to PDPP4T data in [70].

Doping is sometimes known to introduce morphological changes to the ordering within the lattices of organic semiconductors. An increased lattice ordering upon doping has the potential to increase the overall conductivity of the system by boosting the mobility in addition to the carrier concentration. Such a situation is expected to increase σ_{max} within the system. In cases where the mobility is lower on account of reduced ordering, the point of reversal in the conductivity, i.e. σ_{max}, tends to occur at smaller values. Hints of such an observation were seen recently in the case of TrTPFB-doped P3HT [84].

Figure 7 shows polaron model fits to 4 different datasets of $S-\sigma$ available in the literature. In Fig. 7A, a polaronic model fit to $S-\sigma$ is made for doped P3HT [85]. In achieving this fit, $\gamma = 6.1$ and $\sigma_{max} = 150$ S/cm. σ_{max} used here was the maximum seen in experiment, not the point of conductivity trend reversal, since the experiment had not shown this. On the same plot, and for comparision, 2 other recent models, namely, the semi-localized transport (SLoT) model and the Kang–Snyder model, have also been shown [55,85]. It is arguable that the functional form of the scaled polaronic model fits the data over the entire range of conductivities in a manner better than the other 2 used models. Figure 7B shows a fit of the polaronic model to $S-\sigma$ data for poly(3,4-ethylenedioxythiophene) (PEDOT) [85]. Once again, a comparison is made with the SLoT model and the Kang–Snyder model. In the scaled polaron fit, $\gamma = 1.3$ and $\sigma_{max} = 200$ S/cm. All 3 models fit the data reasonably well, although the scaled polarnoic model fits the data better in the regime of very large conductivities too. Figure 7C shows a fit to $S-\sigma$ data of PBTTT [56]. In this scaled polaron fit, $\gamma = 9.0$ and $\sigma_{max} = 600$ S/cm. Lastly, Fig. 7D shows a fit to $S-\sigma$ data of PDPP4T [70]. This dataset is different from that of Fig. 6C in that a commercially available polymer material was used here that has a higher conductivity. In this fit, $\gamma = 4.5$ and $\sigma_{max} = 32$ S/cm. Once again, as in Fig. 6C for PDPP4T, the scaled polaronic model deviates from the data at low conductivites potentially due to a change in the nature of transport. It ought to be highlighted that doped polymers P3HT, PEDOT, and PBTTT all have maximum conductivites over 100 S/cm and often in the several hundreds of S/cm. The doped PDPP4T samples had maximum conductivites below 10 S/cm or in the low tens of

S/cm, so it is conceivable that the transport mechanism at lower conductivities may have a larger contribution from thermally activated hopping or VRH rather than purely from polaronic transport.

In the absence of knowing the simultaneous contributions that influence the lumped dimensionless scaling parameter γ that we have used above, it is difficult to know how this parameter changes depending on tuning specific microscopic material parameters incorporated by other models in the literature. At the moment, we consider, out of conscious intent one must add, γ to be a coarse-level dimensionless scaling parameter that encompasses the microscopics in doped organic materials, and see it as a high-level way to scope out organic thermoelectric materials as will be demonstrated later on in this work. Right now, we only use it to highlight that the polaron model fits the experimental data well over a large range of conductivites, arguably better than existing models on the market, re-iterating the role of mobile polarons within organic thermoelectrics at large carrier densities. A robust $\gamma - \sigma_{max}$ relationship was not found from the 5 datasets analyzed in this work, but what seems clear is that the upper bound on γ is around 10. This is because there is no experimental data in the literature showing that the Seebeck coefficient in organic semiconductors can be below 100 μV/K when its electrical conductivity is below 10^{-3} S/cm. A deeper understanding of the $\gamma - \sigma_{max}$ interrelation may become clear as more experimental data continue to be published. There is also a need for comprehensive $S - \sigma$ experimental datasets from the same laboratory to remove any ambiguity and calibration errors related to how the Seebeck coefficient and the conductivity are extracted from experiment.

To account for the deviant low conductivity behavior in the $S - \sigma$ relationships of PDPP4T, the data in literature have been analyzed using an approach summarized in Fig. 8 [70,86]. Figure 8A shows the measured $S - \sigma$ relationship of PDPP4T published in the original paper. Evidently, the efficiency of doping seems to depend on the temperature at which the doping process was carried out. Improved doping efficiency leads to more ideal behavior at very large conductivities as seen for PDPP4T doped at 75 °C. Figure 8B to D highlights the postulation that the spatial distribution of dopants in the conjugated polymers has a profound impact on the shape of the Seebeck versus conductivity curve, and that it is the clustering of dopants in the polymer that modifies the shape of the DOS and alters the trend of Seebeck versus conductivity curve. Figure 8B and C shows 2 types of densities of states: one a conventional Gaussian with a DOS width of $3k_BT$, and the second a heavy-tailed distribution. The corresponding Seebeck versus conductivity curves shown in Fig. 8D are color coded to correspond to different positions of the Fermi level in the DOS of Fig. 8B and C, below which the DOS is filled. Figure 8D can simulate the reduction in the Seebeck coefficient upon doping quite well, together with the reduced slope on the $S - \sigma$ plot upon doping. However, it does not simulate the point of maximum in the conductivity shown earlier in Fig. 6C of the same work. The study summarized in Fig. 8 attempted to establish that the shape of the $S - \sigma$ curve depends on the clustering of the dopants in the conjugated polymer. The dopant distribution affects the DOS, with dopant clustering dramatically increasing the energetic disorder, which in turn affects charge transport properties. The shallower $S - \sigma$ trends with heterogeneous spatial distributions of dopants in the sample suggested that a heterogeneous distribution of coulombic potentials from doping broadens the DOS and thus depresses the Seebeck coefficient. The modeling that was used to arrive at these conclusions was based on hopping between localized sites with Miller Abrahams hopping rates [86]. The model, although implemented very carefully by the authors, depends on multiple parameters such as the localization length of charge carriers, the jump frequency, an average distance between sites, an externally applied electric field, the dopant cluster density, the number of dopants per cluster, and a few others. From an applied standpoint, it is very difficult to maximize the power factor of the organic thermoelectric material by optimizing multiple variables in such disorder hopping models, some of which can be quantified through experiment and some of which cannot. It is for this reason alone that we have attempted to look at the experimental data of $S - \sigma$ in the literature with an ultra-simplified univariate polaronic model and attempt an understanding of whether $ZT > 1$ may ever be achievable in organic thermoelectrics.

Alternative Explanation for Reduced Slopes on $S - \log(\sigma)$ Plots Based on Hall Mobility Trends

An alternative, quasi-speculative, understanding of why the slopes of the $S - \log(\sigma)$ plots change depending on whether the measurement is done in the nondegenerate regime, or the near-degenerate regime, can be understood from Fig. 9, which collates data published in existing literature [3,57,60,87]. This alternative viewpoint can explain both reduced slopes in $S - \log(\sigma)$ plots and the maxima in the power factor within the highly doped regime. It may be able to connect the measurements of the Seebeck coefficient with measurements of the Hall effect in organic semiconductors in a cohesive fashion. Figure 9A shows the measurement of $S - \log(\sigma)$ for various DPP-based polymers in the nondegenerate and near-degenerate regimes. We have demarcated a boundary around 10 S/cm that divides the 2 regimes, although such a division here is purely for argument's sake and may be variable depending on the material under investigation.

In semiconducting oxide systems exhibiting polaronic transport, such as in Al-doped ZnO, the mobility is observed to increase proportional to an increase in the conductivity. In other words, $\mu \propto \zeta\sigma$, where ζ is a constant of proportionality. When this observation is seen, the slope of $S - \log(\sigma)$ goes from being $-\frac{k_B}{e}\ln(10)$ to being $-\frac{k_B}{e}\ln(10) \times (1 - ne\zeta)$ [81]. Beyond the oxide hopping conductors, such a trend of $\mu \propto \zeta\sigma$ is seen in various F4TCNQ- and TFSI-doped PBTTT polymers [60]. Extracted data from this work are plotted in Fig. 9B. A similar trend was also measured within the ion gel [EMIM][TFSI] gated organic semiconductor C8-DNBDT-NW, again plotted in Fig. 9B [87].

The region of interest in Fig. 9A is the high conductivity regime of several tens of S/cm, not achievable within solid-state organic thin-film transistors. The mobility values shown in Fig. 9B are the measured Hall mobilities. We can extract a proportionality coefficient $\zeta = 0.00413$ cm^3/(S-Vs) for F4TCNQ-doped PBTTT and $\zeta = 0.026$ cm^3/(S-Vs) for ion gel-gated C8-DNBDT from Fig. 9B.

Using the modified Jonker slope of $-\frac{k_B}{e}\ln(10) \times (1 - ne\zeta)$ together with these values of ζ, and with carrier densities $n \sim 2 \times 10^{20}$ cm^{-3} as is the case for both the doped and the ion gel-gated samples, F4TCNQ-doped films will not have much of a reduction in the expected slope since $-\frac{k_B}{e}\ln(10) \times$

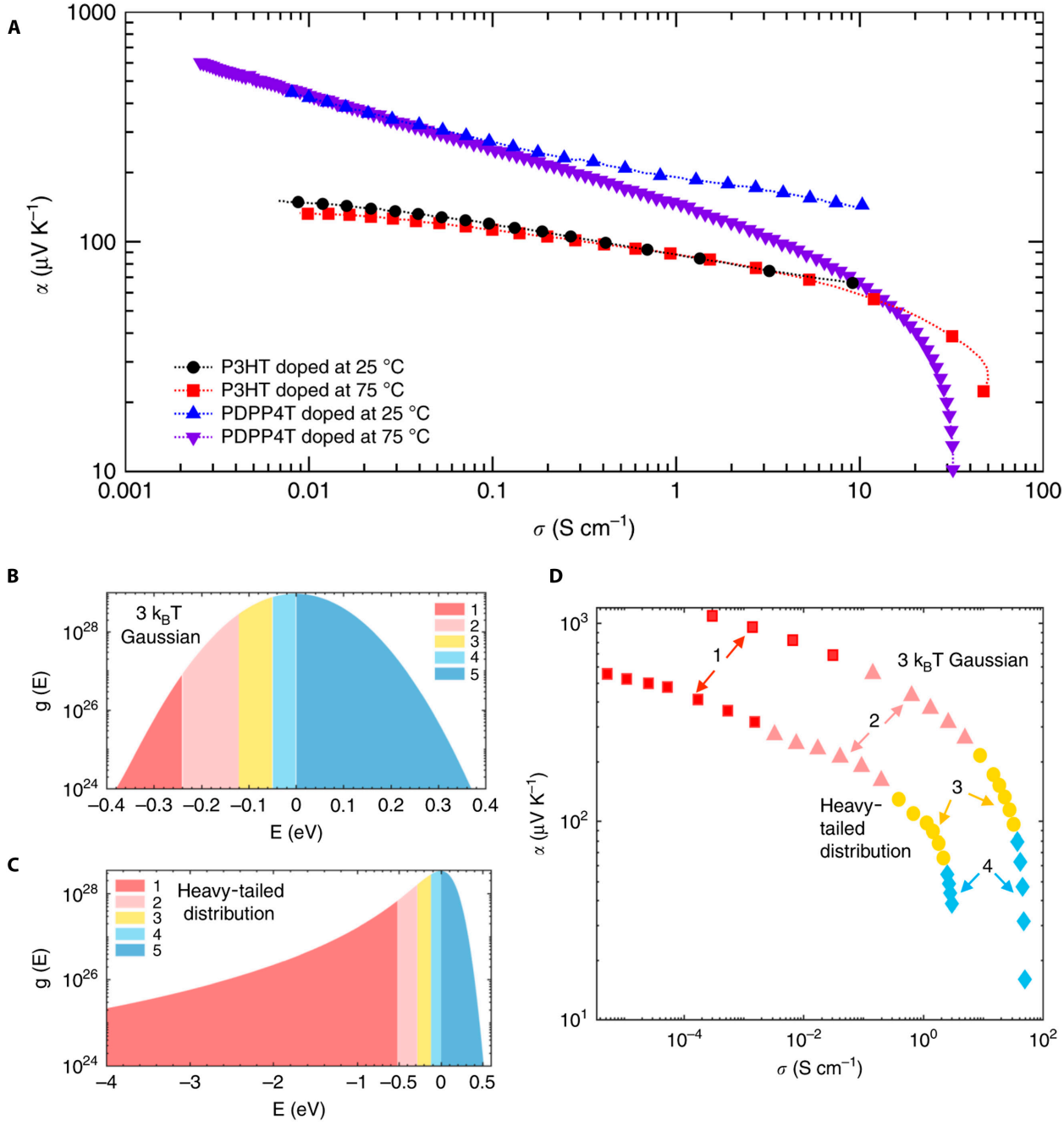

Fig. 8. $S-\sigma$ in PDPP4T and the impact of DOS distribution on $S-\sigma$. (A) $S-\sigma$ experimental data on PDPP4T showing a drastic reduction in the Seebeck coefficient at large conductivities. (B) Schematic showing the filling up of the Gaussian DOS upon doping. (C) Filling up of heavy-tailed DOS with increasing doping by varying the Fermi level E_F further and closer to the center of the energy distribution. (D) Corresponding effect on the log–log plot of Seebeck coefficient versus conductivity. Image taken from [70].

$\left(1-2\times10^{20}\times1.6\times10^{-19}\times0.00413\right)=-0.87\frac{k_B}{e}\ln(10)$, whereas in the ion gel-gated organic semiconductor C8-DNBDT, $-\frac{k_B}{e}\ln(10)\times\left(1-2\times10^{20}\times1.6\times10^{-19}\times0.026\right)=-0.17\frac{k_B}{e}\ln(10)$. $ne\zeta$ is dimensionless since $\mathrm{cm}^{-3}\times\mathrm{C}\times\mathrm{cm}^3/(\mathrm{S\text{-}Vs})$ all cancel out.

In other words, the exact reduced Seebeck–conductivity slope, quantified not by an arbitrary dimensionless γ parameter as done before, but through an experimentally measured ζ parameter in the high conductivity regime, may be justified through a modification of the Jonker slope to the value of $-\frac{k_B}{e}\ln(10)\times(1-ne\zeta)$. The slope may be very much ζ dependent rather than dependent on carrier concentration alone.

When $\mu\propto\zeta\sigma$, the Jonker formula for the Seebeck coefficient, which is originally $S=-\frac{k_B}{e}\left\{-\ln\sigma+\ln\left[e\mu_0N_c\exp(A)\right]\right\}$, calls for modification. It becomes $S=-\frac{k_B}{e}\left\{-\ln\sigma+\ln\left(\mu_0+\zeta\sigma\right)+\ln\left[eN_c\exp(A)\right]\right\}$. All parameters hold their usual meanings in the context of semiconductor thermoelectrics in these

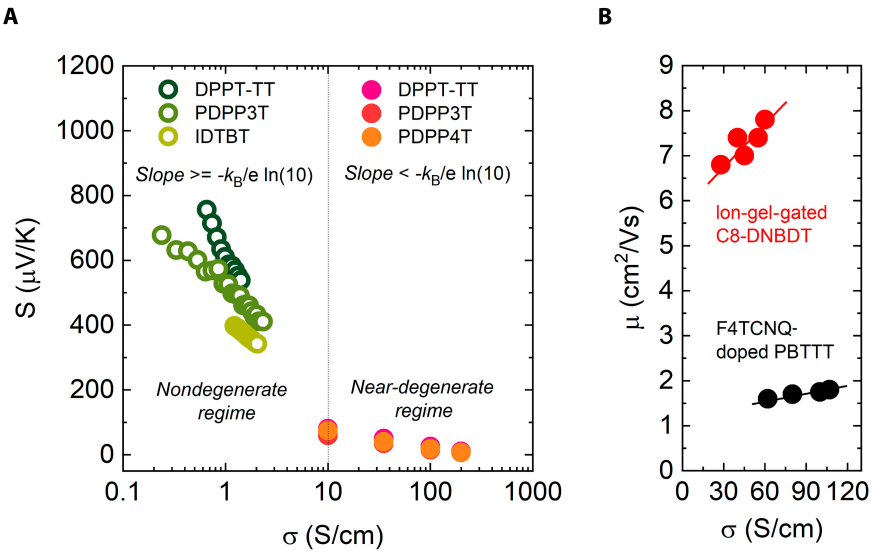

Fig. 9. Relationship between the Seebeck coefficient, mobility, and conductivity. (A) Seebeck coefficient versus conductivity on a linear–log scale. The slope of the Seebeck coefficient versus the conductivity provides an indication of the transport regime, either nondegenerate or near degenerate. (B) The relationship between the mobility and the conductivity in the near-degenerate regime is an indicator of how reduced the slope is in comparison to the nondegenerate Jonker limit of $-\frac{k_B}{e}\ln(10)$.

equations. In simpler terms, the Seebeck coefficient can now be written as $S = \frac{k_B}{e}(1-\mathrm{K}) \times (\ln\sigma - \mathrm{C})$, where K and C are empirical constants. This equation indicates that the Seebeck coefficient measured in such a regime is also reduced in magnitude compared to the original predictions of Jonker's formula for S stated above. Thus, both a smaller magnitude of the Seebeck coefficient and a reduced Seebeck slope are accounted for. Using this equation for the Seebeck coefficient $S = \frac{k_B}{e}(1-\mathrm{K}) \times (\ln\sigma - \mathrm{C})$, a maximum exists in the power factor since taking $\frac{\partial S^2\sigma}{\partial\sigma} = 0$ yields an optimum on the $S^2\sigma$ versus σ plot. In polaronic systems, the relationship between mobility and conductivity, i.e., $\mu \propto \zeta\sigma$, and the magnitude of the proportionality constant ζ may thus be crucial in quantifying the reduction in slopes in an alternative way.

To summarize, in the presence of a sizable ζ [>0.01 cm^3/(S-Vs), for example], and for carrier densities >10^{19} cm^{-3}, the Seebeck slope on the $S-\log(\sigma)$ curve can be smaller in magnitude than $-\frac{k_B}{e}\ln(10)$, and the new "reduced Seebeck slope" is $\frac{\partial S}{\partial\log\sigma} = -\frac{k_B}{e}\ln(10) \times (1 - ne\zeta)$. First evidence for such behavior in a polaronic system was shown in [81]. In the regime of these observations, the power factor of the system also registers a maxima. Quantifying the proportionality constant ζ between the Hall mobility and the conductivity in highly doped organic semiconductors and connecting this proportionality constant with the reduction in the Seebeck coefficient upon increased doping may be a new way to analyze data in the literature in future. Such an analysis may provide an avenue to directly connect the carrier mobility with the Seebeck coefficient in highly doped organic semiconductors, something that is currently lacking. The analysis presented in Fig. 9 is only a guideline at this point. Seeing as Hall mobilities in the DPP polymers are not currently present in the literature, it is difficult to analyze our hypothesis for data presented in Fig. 9A.

Revisiting the Observations Claiming Semiconductor to Metal Transitions, and Metallic Transport, in Measurements of the Seebeck Coefficient in Highly Doped Organic Semiconductors

In previous work that measured the Seebeck coefficient and the electrical conductivity in doped organic semiconductors (reproduced in Fig. 3), a semiconductor to metal transition was claimed to be observed as the carrier density in the system increased from the nondegenerate regime to the near-degenerate regime [54,56,57]. Hints at metallic transport ($S \propto T$) were also seen in measurements of the temperature dependence of the Seebeck coefficient shown in Fig. 4, although the temperature dependence of the conductivity in these doped organic systems still appeared temperature activated [60]. The temperature dependence of the Seebeck coefficient and the temperature dependence of the electrical conductivity have so far never been explained within a single self-consistent framework for organic semiconductors. A prospect at unifying this observation with the other observations in organic thermoelectrics arises within a polaronic transport framework [30]. The work of Emin on small polarons might provide a fertile ground that unifies these seemingly uncorrelated results on carrier hopping and transport in organic semiconductors. Emin believes that in the presence of structural disorder such as in amorphous semiconductors, or where hopping occurs between inequivalent sites, an energy band of small polaron states occurs, resulting in an additional term that is approximately linear in temperature such that $S' = S + \beta T$ [88]. S' is the Seebeck coefficient, S is the standard configurational entropy term, and β is a constant of proportionality. In particular, the overall Seebeck coefficient S' measured for such small polarons is much larger (about tens to few hundreds of μV/K) than the Seebeck expected for a degenerate semiconductor or a metal with a well-defined

Fermi sea (about tens of μV/K) [89]. Linear trends in the Seebeck coefficient with temperature in small polaron systems are indeed seen in materials such as silicon carbide as shown in [88]. A theoretical formalism for the same was shown in [30]. In Emin's own words, "For weakly degenerate small-polaron hopping among a broad distribution of inequivalent sites the Seebeck coefficient is reasonably close to the observed form, $S' = S + \beta T$." The configurational entropy term S reduces with higher carrier concentration, of course. This small polaronic framework may provide one explanation for the discussion around Fig. 4.

On a somewhat related note, polaronic hopping may also be the foundation for what has been referred to in the literature as "band-like transport" for high-mobility organic semiconductors. Since the mobility function for polarons is $\mu = \frac{g(1-c)ea^2\nu}{k_B T}\exp\left(-\frac{E_H}{k_B T}\right)$, at temperatures around 300 K, such a functionality can give rise to an increase in the mobility upon reducing the temperature when the hopping energy is small.

In what follows, we introduce a different conceptual framework to explain trends in the Seebeck coefficient that resemble a semiconductor to metal transition.

For thin polymer films, we consider that the Seebeck coefficient is a function of 2 independent variables, and that charges move in a plane along x and y directions, which are the vector components of the total charge flow. This assumption is justified in materials such as PBTTT with transport anisotropy where charge hopping across the alkyl side chains is small compared to along the backbone plus the π–π stacking direction. By considering that the radial component of this vector can be given in terms of a saturation index, $r = \frac{N-n}{n}$, we propose that the Seebeck coefficient satisfies a diffusion-type equation like the porous medium equation. Given that the underlying process consists of charge transport in a spatially constrained medium, it is natural to propose that the governing equation is like a nonlinear diffusion one, e.g., the porous medium equation [90]. Similar approaches have been used to described charge transport phenomena, particularly in dye-sensitized solar cells [91–93]. In the stationary regime and in the radially symmetric case, this porous medium equation is $\frac{1}{r}\frac{\partial}{\partial r}\left(r\frac{\partial}{\partial r}S^m\right) = C$, where C is a constant in r but may capture temperature dependence. Rearranging this equation leads to $\frac{\partial}{\partial r}\left(r\frac{\partial}{\partial r}S^m\right) = Cr$, and integrating in space gives us $\left(r\frac{\partial}{\partial r}S^m\right) = Cr^2 + C_1$. This equation can be rearranged to give $\frac{\partial}{\partial r}S^m = Cr + C_1\frac{1}{r}$, and integrating in space once again gives us $S^m = Cr^2 + C_1\ln(r) + C_2$.

In the nonsaturated case, i.e., a case of low carrier density, we consider the linear case where the exponent $m = 1$ and that the constant C is small. We thus get $S = C_1\ln(r) + C_2$, which for our chosen saturation index parameter $r = \frac{N-n}{n}$ has the same form for the Seebeck coefficient shown earlier, i.e., $\alpha = \frac{k_B}{e}\ln\left(\frac{N-n}{n}\right) + \frac{k_B}{e}\ln(2) + \alpha_{vib}$.

In the regime of larger carrier densities, we consider higher exponents of m, namely, $m = 3$, that the constant C depends linearly on temperature, and that the constants C_1 and C_2 are small, leading to $S = Cr^{2/3} = C\left(\frac{N}{n} - 1\right)^{2/3}$. By expanding the expression in the parenthesis and keeping the first-order term, we have $S = Cr^{2/3} = CN^{2/3}\left(\frac{1}{n}\right)^{2/3}$. This equation is similar to $S = \frac{8\pi^2 {k_B}^2 T}{3eh^2}m_s^*\left(\frac{\pi}{3n}\right)^{2/3}$, where the effective mass m_s^* is defined as $m_s^* = \left(N_V^* K^*\right)^{2/3} m_c^*$. The respective parameters were defined in the context of thermoelectrics earlier; N_V^* is the effective valley degeneracy, K^* is the effective carrier pocket anisotropy, and m_c^* is the inertial effective mass [94].

What we demonstrate above is that the porous medium equation for polaron diffusion is able to capture the transition of the Seebeck coefficient in its functional form for low carrier density, namely, $S \propto \ln\left(\frac{N-n}{n}\right)$, to a functional form for high carrier density, namely, $S \propto N^{2/3}\left(\frac{1}{n}\right)^{2/3}$. These functional forms are just like those used to justify claims of semiconductor to metal transitions in doped organic semiconductors. We speculate that the accompanying temperature trends in the 2 regimes are captured by the constants in the radial porous medium equation. The complete development of a transport model for the Seebeck coefficient based on the radial porous medium equation goes beyond this review article, but we have taken the opportunity to show briefly how the nondegenerate and the near-degenerate regimes may be characterized by values of the exponent $m = 1$ and $m = 3$, respectively, as these exponents generate functionalities similar to those of a semiconductor to metal transition shown previously in the literature on organic thermoelectrics.

Limitations on *ZT* within a Polaronic Framework of Thermoelectric Transport

With the above discussion laid out based on comprehensive experimental observations in the literature, we proceed to understand whether it is theoretically possible to achieve a figure of merit $ZT \geq 1$ in polaronic hopping systems such as organic semiconductors. It has long been argued that the thermal conductivity, κ, in organic semiconductors is low, hovering at fractions of W m^{-1} K^{-1} [95,96]. These low thermal conductivities are predominantly seen in undoped organic semiconductors or in organic semiconductors within the nondegenerate regime of transport. As the doping in these systems is increased to enter the near-degenerate regime, the total contribution to the thermal conductivity, κ_{total}, comes not only from its phonon contribution, κ_{phonon}, but also from its conductivity-dependent electronic contribution, $\kappa_{electron} = L_0\sigma T$ [97]. L_0 is the Lorentz number, and T is the temperature. Written explicitly, $\kappa_{total} = \kappa_{phonon} + L_0\sigma T$. Considering this equation, the total thermal conductivity in the near-degenerate regime does not profit from the rhetoric that organic semiconductors have low thermal conductivities, which can boost the figure of merit ZT. Figure 10A shows the thermal conductivity of F4TCNQ-doped PBTTT along with a few other organic polymers. It demonstrates that as the electrical conductivity is increased to greater than 10 S/cm, the overall thermal conductivity increases to more than 1 W m^{-1} K^{-1} [97].

In this section, we assume that the electronic contribution to the thermal conductivity in the doped organic semiconductor is ideal and is a function of the Lorentz number $L_0 = 2.44 \times 10^{-8}$ V^2/K^2. In the literature, however, there are varying accounts on the actual value of the Lorentz number in organic semiconductors. In some cases, the Lorentz number was reported to be well above the ideal value of L_0, while in other cases the value

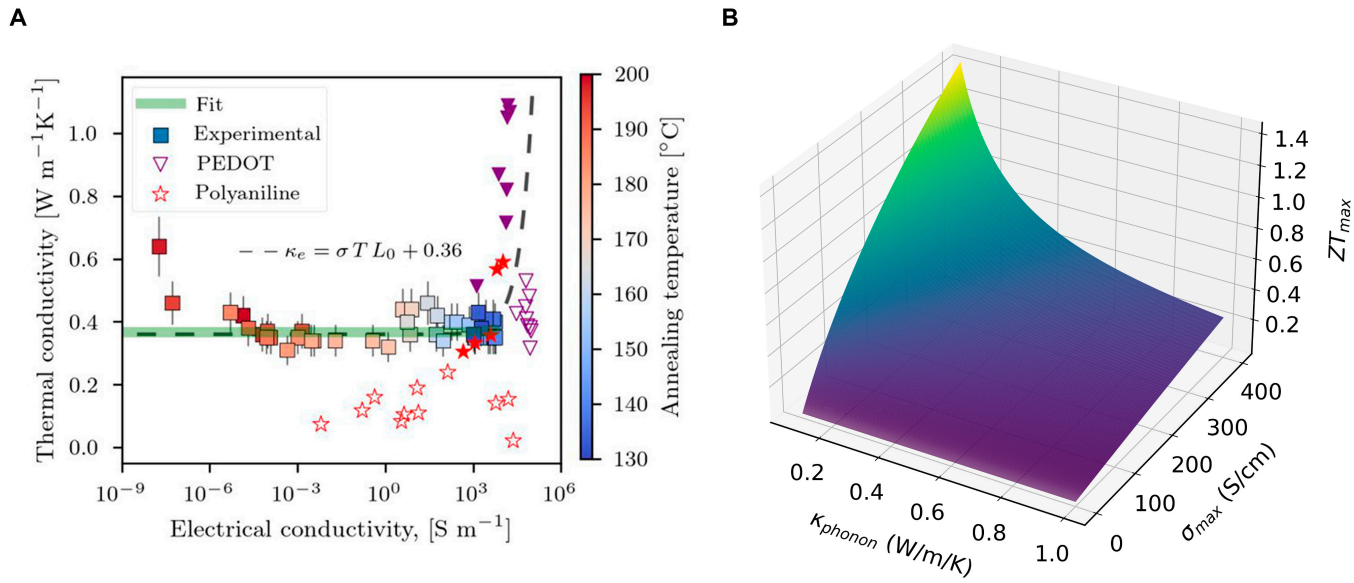

Fig. 10. Thermal conductivity and figure of merit *ZT* in polaronic conductors in the near-degenerate regime. (A) Thermal conductivity in polymers doped to large electrical conductivities in the near-degenerate regime showing a significant increase in the thermal conductivity from its nondegenerate value. (B) *ZT* computed based on the power factor of a polaronic system with free parameters of κ_{phonon} and σ_{max}. This is a best-case scenario for *ZT* with $\gamma = 1$ and is hence called ZT_{max}. Image 10 (A) taken from [97].

was lower [98,99]. In the likelihood that the Lorentz number is nonideal in the case of organic semiconductors, one will need to scale the electronic contribution to the thermal conductivity appropriately in our model.

To compute the maximum *ZT*, we compute the Seebeck coefficient, and the power factor based on the polaronic model deployed earlier in this work. It is known that the scaled power factor exhibits a maxima for large electrical conductivities as shown in Fig. 5C. We multiply this scaled power factor by a variable value for the maximum conductivity and divide it by the total thermal conductivity at 300 K. We then pick out the maximum of the resulting composition. In other words, we compute $ZT = S^2\sigma_{norm}\sigma_{max}/(\kappa_{phonon} + L_0\sigma_{norm}\sigma_{max}T)$ for $T = 300$ K, plot $S^2\sigma_{norm}\sigma_{max}/(\kappa_{phonon} + L_0\sigma_{norm}\sigma_{max}T)$ versus $\sigma_{norm}\sigma_{max}$, and extract the maximum value for *ZT* on this plot. These values are what we call ZT_{max} and are plotted on Fig. 10B as a function of κ_{phonon} and σ_{max}. As is evident from Fig. 10B, a $ZT_{max} \geq 1$ is possible only for $\kappa_{phonon} < 0.2$ W m^{-1} K^{-1} and $\sigma_{max} > 300$ S/cm. These values represent the most ideal case. σ_{max}, it must be re-iterated again, is the measured value of conductivity at the point of trend reversal on the $S - \sigma$ plot in the near-degenerate regime of polaron transport (see Fig. 5A for a reminder).

The above having been said, upon entering the near-degenerate regime where σ_{max} is a few hundreds of S/cm (see Fig. 7), we must account for the dimensionless factor γ to scale the Seebeck coefficient. This implies that the measured value of the figure of merit *ZT* reduces to ZT_{max}/γ^2 in the near-degenerate regime. For $\gamma = 9$, as is the case for highly doped PBTTT with $\sigma_{max} = 600$ S/cm shown in Fig. 7, this leads to the value of ZT_{max} on Fig. 10B needing to be divided by 81. In other words, an expectation of $ZT_{max} = 1$ upon efficient doping of the polymer will only lead to $ZT \approx 0.01$ in practice.

This is potentially the reason why some of the highest *ZT* values observed in organic polymers have not been seen in the degenerately doped regime. For example, the n-type fullerene-based organic material, doped PTEG-2, has shown a *ZT* around 0.3 with a conductivity little over 10 S/cm, a Seebeck coefficient around −250 μV K^{-1}, and a thermal conductivity of less than 0.1 W m^{-1} K^{-1} [100]. In Fig. 10B, such values correspond to around 0.3 (assuming of course that σ_{max} for doped fullerenes cannot be as high as for the doped polythiophenes).

In the doped polymer PEDOT-tosylate, $ZT = 0.25$ was experimentally observed for conductivity around 100 S/cm, a Seebeck coefficient around 200 μV K^{-1}, and a thermal conductivity of 0.37 W m^{-1} K^{-1} [101]. We showed that doped PEDOT shows a small $\gamma = 1.3$ (see Fig. 7B) much smaller than any of the other polymers studied herein. Because of this small γ, the reduction in *ZT* upon doping into the high conductivity regime is not as much as it is for the other polymers. Looking at Fig. 10B, one finds that the values of PEDOT correspond to $ZT_{max} \approx 0.22$. Even upon slight reduction by a factor of γ^2, the polaron model prediction is not too far off from the measured value.

For $ZT_{max} \geq 1$, one needs to look for 3 properties in doped organic polymers: (a) a Seebeck coefficient–conductivity relationship that is nearly ideal ($\gamma = 1$) within the near-degenerate regime, (b) a σ_{max} value extracted in the near-degenerate regime (at the point of conductivity reversal) of several hundred S/cm, and (c) a low phonon contribution κ_{phonon} below 0.2 W m^{-1} K^{-1}. Judging purely from the experimental trends currently in the literature and in reading the story they tell us over the backdrop of polaronic transport, it may be challenging to achieve ZT_{max} (and hence *ZT*) ≥ 1 for power generation purposes using single layers of organic polymers.

Organic crystalline radical ion salts and organic small molecules are governed by alternative transport mechanisms, which are known to push the experimental value of *ZT* beyond 0.1 [102]. Although the morphology of these films plays a crucial role in their power conversion efficiency [103], theoretical calculations on such materials have shown that $ZT \geq 1$ may indeed be possible [104]. This class of materials may thus provide some light at the end of the tunnel for organic thermoelectrics, superseding polaronic organic polymers.

Even if not considering the role of mobile polarons in transport, there is emerging consensus that the field of organic thermoelectrics has hit a roadblock, and that the pathway to improving the thermoelectric figure of merit beyond 1 is not as simple as pursuing brute force doping strategies to increase the electrical conductivity [105]. It is also still not clear as to what range the transport parameters σ, S, and κ can be controlled over, and whether they can be tuned independent of each other. This is down to several reasons, 3 of which are summarized here. First, the active layer morphology may or may not be perturbed by the incorporation of dopant molecules. Second, ionized dopants in the host may contribute to Coulomb scattering and charge carrier trapping. Third, the formation of bipolarons upon doping may be a detriment, as bipolarons can be either immobile or less mobile compared to single polarons.

A few strategies have been proposed to overcome the existing roadblocks. One strategy is that of modulation doping, bottom-up, where dopants preferentially sit in an amorphous phase, and the actual charge transport occurs in a crystalline phase [106]. The crystalline phase is thus unaltered in its microstructure, and there is a spatial separation between dopants and mobile charges. A second strategy is that of dopant alignment, or intentional and directional dopant clustering [105,107].

Both these techniques may enable polaronic transport with a pure number $\gamma = 1$. Under modulation doping, for example, the relationship between S and σ for the polarons that participate in transport will not be affected by the simultaneous effects of disorder introduced upon doping and can thus be considered ideal. The measured value of ZT will not need to be scaled down and will approach the value of ZT_{max} in our model. These suggested that doping strategies may thus bring $ZT = 1$ consistently within reach. While our work predominantly focuses on the properties of individual layers of organic semiconductors, and their ability to show increased ZT, it must be mentioned that newer approaches based on polymeric multi-heterojunctions have been used recently to successfully demonstrate $ZT > 1$ [108].

Applications of Organic Thermoelectrics beyond Power Generation

Although the field of organic thermoelectrics continues to be studied with much intensity for applications in power generation, there are several emerging applications that make use of their attractive thermoelectric properties that go well beyond ZT optimization. Three applications can be immediately highlighted. First, advanced thermoelectric devices based on polymers have been used in very fast heat sensors. Under infrared (IR) irradiation at specific wavelengths, chosen molecular vibrational modes in organic polymers can be excited, opening a pathway for fast heat transport within molecular films [109]. The prospect of exciting molecular vibrations under IR resonance is a promising pathway to use organic semiconductors in future ultrafast bolometers. Second, the relatively low thermal conductivity within undoped or gated organic transistors can be used to monitor thermal runaway and device degradation under operational conditions [110]. Third, low thermal conductivities can also be used in devices to detect radiation. One such thermoelectric radiation sensor (TESS) is shown in Fig. 11.

Figure 11A shows a functionally integrated TESS, replete with a thermoelectric element and a high-speed operational amplifier with 100-fold gain. The circular disc mounted on a

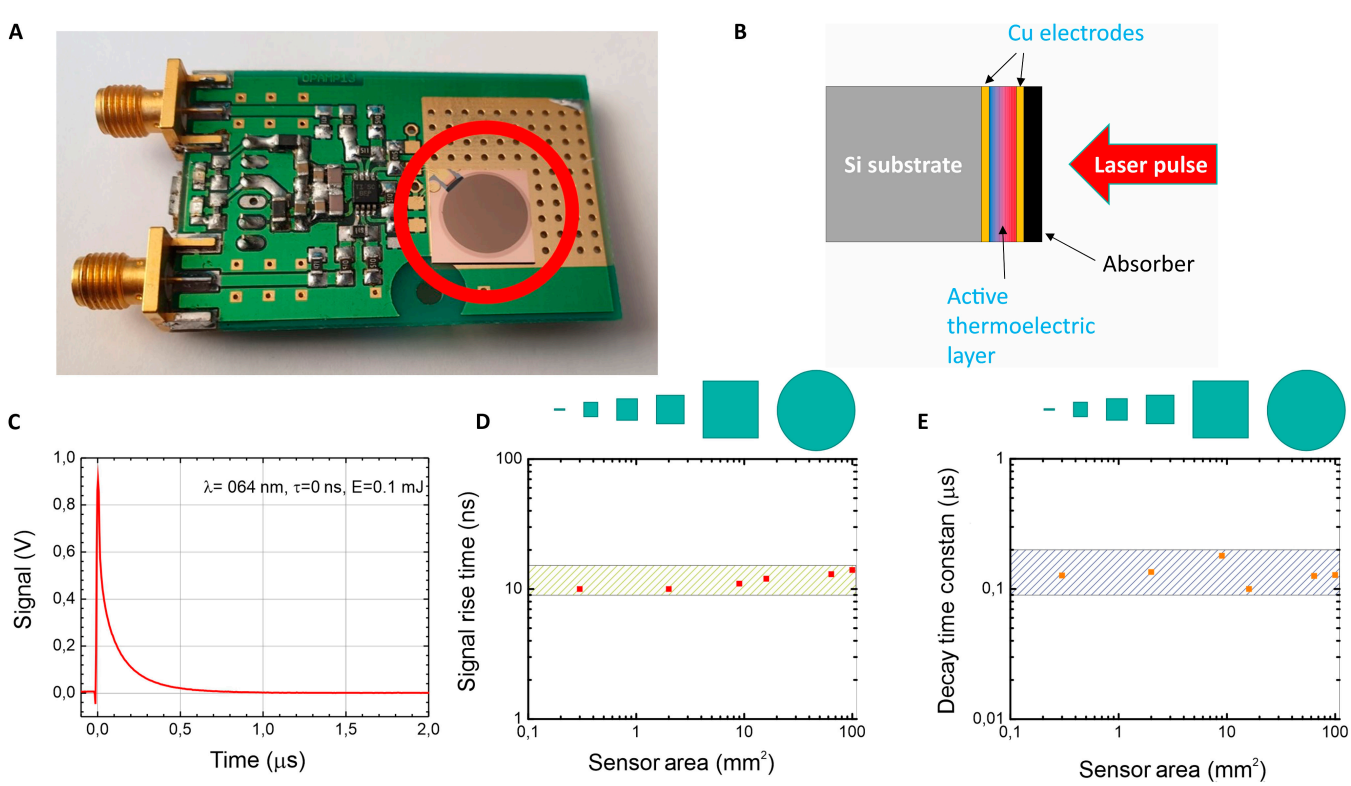

Fig. 11. TESS based on organic semiconductors licensed out to Thorlabs in 2022. (A) Fully integrated TESS based on an organic small-molecule film. (B) Schematic diagram of the sensor element showing the different layers involved. (C) Fast rise time of the sensor upon laser pulse impingement. (D) Area-independent rise time of TESS. (E) Area-independent decay time of TESS.

printed circuit board of the sensor constitutes the thermoelectric element. The cross-section of layers of this element is shown in Fig. 11B. They comprise an absorber that coats a sandwich structure of 2 Cu electrodes and an organic small-molecule film of tetrathiotetracene. This tetrathiotetracene film has a thickness in the hundreds of nanometers to a few micrometers, a Seebeck coefficient greater than 1 mV/K, and a thermal conductivity less than 0.1 W m^{-1} K^{-1}. The sensor element is built within a single vacuum chamber using a sequential deposition of layers with thermal evaporation. The sensor operation principle is based on heat generation at the top Cu electrode when a laser pulse impacts the sensor and is absorbed. This heat dissipates through the organic sandwiched layer, but a voltage spike shown in Fig. 11C develops initially on account of the sensor's low thermal conductivity. The sensor operates in a wavelength range between 0.18 and 2.3 μm without the need for an absorber. However, with the use of an absorber, the wavelength range can be extended to include the CO_2 laser wavelength of 10.6 μm. Additionally, the absorption layer can be tailored to suit a particular spectral region for a specific application if the absorbed radiation can be converted into heat. As a result, the sensor covers a wide range of applications, spanning ultraviolet (UV) to IR. The nanosecond rise time of the voltage signal, shown in Fig. 11D, is both fast and independent of sensor area. The decay time, shown in Fig. 11E, is also area independent. This feature permits the TESS to be scaled to much larger areas on the centimeter scale for radiation detection as required. The large area scalability of the sensor is a positive contrast to photodiodes that are typically pinpoint. The area-independent feature is a consequence of heat transport through the film in the vertical direction, perpendicular to the device stack. The 3-fold unique selling point of this TESS is that it is fast, it operates over a broad spectral range, and it can be scaled in area, making it independent of size. The TESS technology was licensed out to Thorlabs for commercialization in 2022. It is a significant demonstration of the tremendous innovative potential that organic thermoelectrics has for novel applications, not reliant on ZT.

Summary

This work was an attempt to consolidate the experimental findings in the field of organic thermoelectrics under a unified framework based on polaronic hopping. We highlighted the salient measurements within the literature on organic thermoelectrics, and rather than just summarize them as is customary in review articles, we attempted to link the observations with each other to build a unified picture. The Seebeck coefficient and the electrical conductivity as functions of carrier density and temperature were first laid out, and the story they tell was constructed based on knowledge of how polarons behave in disordered oxide semiconductors. A plausible unifying explanation was arrived at to justify the observed association between the Seebeck coefficient and the conductivity in both a nondegenerate limit of low conductivity and a near-degenerate limit of high conductivity. The idea of this work was not to build yet another model to explain the data in the literature. Rather, it was to use intuition together with a highly simplified univariate model where the complex physics of disordered thermoelectric transport is compacted into one dimensionless quantity γ. This γ parameter can be extracted directly from measurements of $S - \sigma$, making scoping easier. Observations in the literature point at there being a finite value of γ between 1 and 10. To achieve $ZT = 1$, one would need a low value of γ closer to 1. Beyond ZT optimization and applications in power generation, several new applications continue to emerge, which use the properties of organic semiconductors in new and novel thermoelectric devices. Few applications were highlighted herein, which include thermoelectric radiation sensing, thermal runaway monitoring, and ultrafast bolometers based on molecular resonances. The intrinsic limitations of organic thermoelectrics when it comes to power generation do not apply to newer promising fronts of thermoelectric development.

Acknowledgments

D.V. acknowledges valuable discussions with D. Venkataraman (University of Massachusetts Amherst), Z. Aksamija (University of Utah), H. Tanaka (Nagoya University), and H. Sirringhaus (University of Cambridge) in the preparation of this manuscript.
Funding: D.V. also acknowledges the Royal Society for funding in the form of a Royal Society University Research Fellowship (Royal Society Reference No. URF/R1/201590). G.S. is a Belgian National Fund for Scientific Research (FNRS) Research Associate. G.S. acknowledges financial support from the Francqui Foundation (Francqui Start-Up Grant) and thanks the FNRS for financial support through research project COHERENCE2 (no. F.4536.23). D.V. and G.S. acknowledge the Wiener-Anspach Foundation (FWA) for support of the ZT1 research project initiated in 2024. The ZT1 project aims to demonstrate $ZT = 1$ figure of merit in organic thermoelectrics.
Competing interests: The authors declare that they have no competing interests.

References

1. Kang K, Schott S, Venkateshvaran D, Broch K, Schweicher G, Harkin D, Jellett C, Nielsen CB, McCulloch I, Sirringhaus H. Investigation of the thermoelectric response in conducting polymers doped by solid-state diffusion. *Mater Today Phys*. 2019;8:112–122.
2. Venkateshvaran D, Nikolka M, Sadhanala A, Lemaur V, Zelazny M, Kepa M, Hurhangee M. Approaching disorder-free transport in high-mobility conjugated polymers. *Nature*. 2014;515(7527):384–388.
3. Broch K, Venkateshvaran D, Lemaur V, Olivier Y, Beljonne D, Zelazny M, Nasrallah I, Harkin DJ, Statz M, Di Pietro R, et al. Measurements of ambipolar Seebeck coefficients in high-mobility diketopyrrolopyrrole donor–acceptor copolymers. *Adv Electron Mater*. 2017;3(11):1700225.
4. Venkateshvaran D, Kronemeijer AJ, Moriarty J, Emin D, Sirringhaus H. Field-effect modulated Seebeck coefficient measurements in an organic polymer using a microfabricated on-chip architecture. *APL Mater*. 2014;2(3):Article 032102.
5. Lee J, Kaake LG, Cho JH, Zhu X-Y, Lodge TP, Frisbie CD. Ion gel-gated polymer thin-film transistors: Operating mechanism and characterization of gate dielectric capacitance, switching speed, and stability. *J Phys Chem C*. 2009;113(20):8972–8981.
6. Harada T, Ito H, Ando Y, Watanabe S, Tanaka H, Kuroda S-I. Signature of the insulator–metal transition of a

semicrystalline conjugated polymer in ionic-liquid-gated transistors. *Appl Phys Express*. 2015;8(2):Article 021601.
7. Tanaka H, Nishio S, Ito H, Kuroda SI. Microscopic signature of insulator-to-metal transition in highly doped semicrystalline conducting polymers in ionic-liquid-gated transistors. *Appl Phys Lett*. 2015;107(24): Article 243302.
8. Kang K, Watanabe S, Broch K, Sepe A, Brown A, Nasrallah I, Nikolka M, Fei Z, Heeney M, Matsumoto D, et al. 2D coherent charge transport in highly ordered conducting polymers doped by solid state diffusion. *Nat Mater*. 2016;15(8):896–902.
9. Ghosh R, Spano FC. Excitons and polarons in organic materials. *Acc Chem Res*. 2020;53(10):2201–2211.
10. Franchini C, Reticcioli M, Setvin M, Diebold U. Polarons in materials. *Nat Rev Mater*. 2021;6(7):560.
11. Bredas JL, Street GB. Polarons, bipolarons, and solitons in conducting polymers. *Acc Chem Res*. 1985;18(10):309–315.
12. Emin D. *Polarons*. Cambridge: Cambridge University Press; 2013.
13. Austin I, Mott NF. Polarons in crystalline and non-crystalline materials. *Adv Phys*. 1969;18(71):41.
14. Junior MLP, Júnior RTS, Silvaa GM, Júnior LAR. Stationary polaron properties in organic crystalline semiconductors. *Phys Chem Chem Phys*. 2019;21(5):2727–2733.
15. Sato H, Rahman SAA, Yamada Y, Ishii H, Yoshida H. Conduction band structure of high-mobility organic semiconductors and partially dressed polaron formation. *Nat Mater*. 2022;21(8):910–916.
16. Hulea IN, Fratini S, Xie H, Mulder CL, Iossad NN, Rastelli G, Ciuchi S, Morpurgo AF. Tunable Fröhlich polarons in organic single-crystal transistors. *Nat Mater*. 2006;5(12):982–986.
17. Kemeny G, Rosenberg B. Small polarons in organic and biological semiconductors. *J Chem Phys*. 1970;53:3549.
18. Lu N, Li L, Geng D, Liu M. A review for polaron dependent charge transport in organic semiconductor. *Org Electron*. 2018;61:223–234.
19. Zheng W, Sun B, Li D, Gali SM, Zhang H, Fu S, Virgilio LD, Li Z, Yang S, Zhou S, et al. Band transport by large Fröhlich polarons in MXenes. *Nat Phys*. 2022;18(5):544–550.
20. Liu Y, Shi W, Zhao T, Wang D, Shuai Z. Boosting the Seebeck coefficient for organic coordination polymers: Role of doping-induced polaron band formation. *J Phys Chem Lett*. 2019;10(10):2493–2499.
21. Emin D. Small polarons. *Phys Today*. 1982;35(6):34.
22. Png R-Q, Ang MCY, Teo M-H, Choo K-K, Tang CG, Belaineh D, Chua L-L, Ho PKH. Madelung and Hubbard interactions in polaron band model of doped organic semiconductors. *Nat Commun*. 2016;7:11948.
23. Chen Y, Ghosh S, Liu X, Zozoulenko IV, Fahlman M, Braun S. Experimental and theoretical investigation into the polaron structure of K-doped polyfluorene films. *J Phys Chem C*. 2021;125(1):937–945.
24. Tietze ML, Benduhn J, Pahner P, Nell B, Schwarze M, Kleemann H, Krammer M, Zojer K, Vandewal K, Leo K. Elementary steps in electrical doping of organic semiconductors. *Nat Commun*. 2018;9(1):1182.
25. Bredas JL, Themans B, Andre J, Chance RR. The role of mobile organic radicals and ions (solitons, polarons and bipolarons) in the transport properties of doped conjugated polymers. *Synth Met*. 1984;9(2):265–274.
26. Scheunemann D, Jarsvall E, Liu J, Beretta D, Fabiano S, Caironi M, Kemerink M, Muller C. Charge transport in doped conjugated polymers for organic thermoelectrics. *Chem Phys Rev*. 2022;3:Article 021309.
27. Watanabe S, Ando K, Kang K, Mooser S, Vaynzof Y, Kurebayashi H, Saitoh E, Sirringhaus H. Polaron spin current transport in organic semiconductors. *Nat Phys*. 2014;10(4):308–313.
28. Salzmann I, Heimel G, Oehzelt M, Winkler S, Koch N. Molecular electrical doping of organic semiconductors: Fundamental mechanisms and emerging dopant design rules. *Acc Chem Res*. 2016;49(3):370–378.
29. Ge Y, Liu R, Suhai Z. Abnormal Seebeck effect in doped conducting polymers. *Appl Phys Lett*. 2021;118(12): Article 123301.
30. Emin D. Thermoelectric power due to electronic hopping motion. *Phys Rev Lett*. 1975;35(13):882.
31. Emin D, Holstein T. Studies of small-polaron motion IV. Adiabatic theory of the hall effect. *Ann Phys*. 1969;53(1): 439–520.
32. Emin D. Generalized adiabatic polaron hopping: Meyer-Neldel compensation and Poole-Frenkel behavior. *Phys Rev Lett*. 2008;100(16):Article 166602.
33. Emin D, Bussac M-N. Disorder-induced small-polaron formation. *Phys Rev B*. 1994;49(20):14290.
34. Emin D. Determining a hopping polaron's bandwidth from its Seebeck coefficient: Measuring the disorder energy of a non-crystalline semiconductor. *J Appl Phys*. 2016;119(4):Article 045101.
35. Nell J, Wood BJ, Dorris SE, Mason TO. Jonker-type analysis of small polaron conductors. *J Solid State Chem*. 1989;82(2):247.
36. D. Venkateshvaran, Seebeck coefficient in organic semiconductors [thesis]. [Cambridge (UK)]: University of Cambridge; 2014.
37. Zhao W, Ding J, Zou Y, Di C-A, Zhu D. Chemical doping of organic semiconductors for thermoelectric applications. *Chem Soc Rev*. 2020;49(20):7210–7228.
38. Scaccabarozzi AD, Basu A, Anies F, Liu J, Zapata-Arteaga O, Warren R, Firdaus Y, Nugraha MI, Lin Y, Campoy-Quiles M, et al. Doping approaches for organic semiconductors. *Chem Rev*. 2022;122:4420–4492.
39. Yuen JD, Dhoot AS, Namdas EB, Coates NE, Heeney M, McCulloch I, Moses D, Heeger AJ. Electrochemical doping in electrolyte-gated polymer transistors. *J Am Chem Soc*. 2007;129(46):14367–14371.
40. Tang H, Liang Y, Liu C, Hu Z, Deng Y, Guo H, Yu Z, Song A, Zhao H, Zhao D, et al. A solution-processed n-type conducting polymer with ultrahigh conductivity. *Nature*. 2022;611(793):271–277.
41. Pernstich KP, Roessner B, Batlogg B. Field-effect-modulated Seebeck coefficient in organic semiconductors. *Nat Mater*. 2008;7(4):321–325.
42. Germs WC, Guo K, Janssen RAJ, Kemerink M. Unusual thermoelectric behavior indicating hopping to bandlike transition in pentacene. *Phys Rev Lett*. 2012;109(1): Article 016601.
43. Overhof H, Beyer W. A model for the electronic transport in hydrogenated amorphous silicon. *Philos Mag B*. 1981;43(3):433–450.
44. Dobryden I, Korolkov VV, Lemaur V, Waldrip M, Un H-I, Simatos D, Spalek LJ, Jurchescu OD, Olivier Y, Claesson PM, et al. Dynamic self-stabilization in the electronic and nanomechanical properties of an organic polymer semiconductor. *Nat Commun*. 2022;13(1):3076.

45. Zhang X, Hugo B, Kronemeijer AJ, Smith J, Kim Y, Kline RJ, Richter LJ, Anthopoulos TD, Sirringhaus H, Song K. Molecular origin of high field-effect mobility in an indacenodithiophene–benzothiadiazole copolymer. *Nat Commun*. 2013;4:2238.
46. DeLongchamp DM, Kline RJ, Lin EK, Fischer DA, Richter LJ, Lucas LA, Heeney M, McCulloch I, Northrup JE. High carrier mobility polythiophene thin films: Structure determination by experiment and theory. *Adv Mater*. 2007;19(6):833–837.
47. Statz M, Venkateshvaran D, Jiao X, Schott S, McNeill CR, Emin D, Sirringhaus H, Di Pietro R. On the manifestation of electron-electron interactions in the thermoelectric response of semicrystalline conjugated polymers with low energetic disorder. *Commun Phys*. 2018;1(1):16.
48. von Mühlenen A, Errien N, Schaer M, Bussac M-N, Zuppiroli L. Thermopower measurements on pentacene transistors. *Phys Rev B*. 2007;75(11):Article 115338.
49. Warwick CN, Venkateshvaran D, Sirringhaus H. Accurate on-chip measurement of the Seebeck coefficient of high mobility small molecule organic semiconductors. *APL Mater*. 2015;3(9):Article 096104.
50. Aselage TL, Emin D, McCready SS, Duncan RV. Large enhancement of boron carbides' Seebeck coefficients through vibrational softening. *Phys Rev Lett*. 1998;81(11):2316–2319.
51. Ito M, Yamashita Y, Mori T, Ariga K, Takeya J, Watanabe S. Band mobility exceeding 10 $cm^2 V^{-1} s^{-1}$ assessed by field-effect and chemical double doping in semicrystalline polymeric semiconductors. *Appl Phys Lett*. 2021;119(1):Article 013302.
52. Yamashita Y, Tsurumi J, Kurosawa T, Ueji K, Tsuneda Y, Kohno S, Kempe H, Kumagai S, Okamoto T, Takeya J, et al. Supramolecular cocrystals built through redox-triggered ion intercalation in π-conjugated polymers. *Commun Mater*. 2021;2(1):45.
53. Yamashita Y, Tsurumi J, Ohno M, Fujimoto R, Kumagai S, Kurosawa T, Okamoto T, Takeya J, Watanabe S. Efficient molecular doping of polymeric semiconductors driven by anion exchange. *Nature*. 2019;572(7771):634–638.
54. Ito H, Mada H, Watanabe K, Tanaka H, Takenobu T. Charge transport and thermoelectric conversion in solution-processed semicrystalline polymer films under electrochemical doping. *Commun Phys*. 2021;4(1):8.
55. Kang SD, Snyder GJ. Charge-transport model for conducting polymers. *Nat Mater*. 2017;16:252–257.
56. Tanaka H, Kanahashi K, Takekoshi N, Mada H, Ito H, Shimoi Y, Ohta H, Takenobu T. Thermoelectric properties of a semicrystalline polymer doped beyond the insulator-to-metal transition by electrolyte gating. *Sci Adv*. 2020;6(7):eaay8065.
57. Kanahashi K, Noh Y-Y, Park W-T, Yang H, Ohta H, Tanaka H, Takenobu T. Charge and thermoelectric transport mechanism in donor-acceptor copolymer films. *Phys Rev Res*. 2020;2(4):Article 043330.
58. Ito S-I, Kanahashi K, Ohta H, Ito H, Takenobu T, Tanaka H. Structure and thermoelectric properties of electrochemically doped polythiophene thin films: Effect of side chain density. *Appl Phys Lett*. 2021;119(18):Article 183304.
59. Russ B, Glaudell A, Urban JJ, Chabinyc ML, Segalman RA. Organic thermoelectric materials for energy harvesting and temperature control. *Nat Rev Mater*. 2016;1(10):16050.
60. Watanabe S, Ohno M, Yamashita Y, Terashige T, Okamoto H, Takeya J. Validity of the Mott formula and the origin of thermopower in pi-conjugated semicrystalline polymers. *Phys Rev B*. 2019;100(24):Article 241201.
61. Dorris SE, Mason TO. Electrical properties and cation valencies in Mn_3O_4. *J Am Ceram Soc*. 1988;71(5):379–385.
62. Tuller HL, Nowick AS. Small polaron electron transport in reduced CeO_2 single crystals. *J Phys Chem Solids*. 1977;38(8):859–867.
63. Ingram BJ, Mason TO, Asahi R, Park KT, Freeman AJ. Electronic structure and small polaron hole transport of copper aluminate. *Phys Rev B*. 2001;64(15):Article 155114.
64. Liang Z, Choi HH, Luo X, Liu T, Abtahi A, Ramasamy US, Hitron JA, Baustert KN, Hempel JL, Boehm AM, et al. n-type charge transport in heavily p-doped polymers. *Nat Mater*. 2021;20(4):518–524.
65. Jonker GH. The application of combined conductivity and Seebeck-effect plots for the analysis of semiconductor properties. *Philips Res Rep*. 1968;23:131–138.
66. Chaikin PM, Beni G. Thermopower in the correlated hopping regime. *Phys Rev B*. 1976;13(2):647.
67. Heikes RR, Ure RW. *Thermoelectricity: Science and engineering*. New York (NY): Interscience Publishers; 1961.
68. Heikes RR, Maradudin AA, Miller RC. Une étude des propriétés de transport des semiconducteurs de valence mixte. *Ann Phys (Paris)*. 1963;8(8):783.
69. Bubnova O, Khan ZU, Wang H, Braun S, Evans DR, Fabretto M, Hojati-Talemi P, Dagnelund D, Arlin J-B, Geerts YH, et al. Semi-metallic polymers. *Nat Mater*. 2014;13:190–194.
70. Boyle CJ, Upadhyaya M, Wang P, Renna LA, Lu-Díaz M, Jeong SP, Hight-Huf N, Korugic-Karasz L, Barnes MD, Aksamija Z, et al. Tuning charge transport dynamics via clustering of doping in organic semiconductor thin films. *Nat Commun*. 2019;10(1):2827.
71. Blackburn JL, Kang SD, Roos MJ, Norton-Baker B, Miller EM, Ferguson AJ. Intrinsic and extrinsically limited thermoelectric transport within semiconducting single-walled carbon nanotube networks. *Adv Electron Mater*. 2019;5(11):1800910.
72. Abutaha A, Kumar P, Yildirim E, Shi W, Yang S-W, Wu G, Hippalgaonkar K. Correlating charge and thermoelectric transport to paracrystallinity in conducting polymers. *Nat Commun*. 2020;11(1):1737.
73. Birch SW, Pipe KP. Effects of dynamic disorder on thermoelectric transport in soft materials. *J Appl Phys*. 2022;131(13):Article 135104.
74. Fritzsche H. A general expression for the thermoelectric power. *Solid State Commun*. 1971;9(21):1813–1815.
75. Hung NT, Nugraha ART, Saito R. Thermoelectric properties of carbon nanotubes. *Energies*. 2019;12(23):4561.
76. Mateeva N, Niculescu H, Schlenoff J, Testardi LR. Correlation of Seebeck coefficient and electric conductivity in polyaniline and polypyrrole. *J Appl Phys*. 1998;83(6):3111.
77. Zhang X, Bu Z, Shi X, Chen Z, Lin S, Shan B, Wood M, Snyder A, Chen L, Snyder GJ, et al. Electronic quality factor for thermoelectrics. *Sci Adv*. 2020;6(46):eabc0726.
78. Statz M, Schneider S, Berger FJ, Lai L, Wood WA, Abdi-Jalebi M, Leingang S, Himmel H-J, Zaumseil J, Sirringhaus H. Charge and thermoelectric transport in polymer-sorted semiconducting single-walled carbon nanotube networks. *ACS Nano*. 2020;14(11):15552–15565.
79. Felizco JC, Uenuma M, Ishikawa Y, Uraoka Y. Optimizing the thermoelectric performance of InGaZnO thin films

depending on crystallinity via hydrogen incorporation. *Appl Surf Sci*. 2020;527:Article 146791.
80. Fujimoto Y, Uenuma M, Ishikawa Y, Uraoka Y. Analysis of thermoelectric properties of amorphous InGaZnO thin film by controlling carrier concentration. *AIP Adv*. 2015;5(9):Article 097209.
81. Kinemuchi Y, Ito C, Kaga H, Aoki T, Watari K. Thermoelectricity of Al-doped ZnO at different carrier concentrations. *J Mater Res*. 2007;22(7):1942.
82. Abdalla H, Zuo G, Kemerink M. Range and energetics of charge hopping in organic semiconductors. *Phys Rev B*. 2017;96(24):241202(R).
83. Kang SD, Dylla M, Snyder GJ. Thermopower-conductivity relation for distinguishing transport mechanisms: Polaron hopping in CeO_2 and band conduction in $SrTiO_3$. *Phys Rev B*. 2018;97(23):Article 235201.
84. Guo J, Chen P-A, Yang S, Wei H, Liu Y, Xia J, Chen C, Chen H, Wang S, Li W, et al. Dopant-induced morphology of organic semiconductors resulting in high doping performance. *Small Methods*. 2024;2400084.
85. Gregory SA, Hanus R, Atassi A, Rinehart JM, Wooding JP, Menon AK, Losego MD, Snyder GJ, Yee SK. Quantifying charge carrier localization in chemically doped semiconducting polymers. *Nat Mater*. 2021;20(10): 1414–1421.
86. Upadhyaya M, Boyle CJ, Venkataraman D, Aksamija Z. Effects of disorder on thermoelectric properties of semiconducting polymers. *Sci Rep*. 2019;9:5820.
87. Kasuya N, Tsurumi J, Okamoto T, Watanabe S, Takeya J. Two-dimensional hole gas in organic semiconductors. *Nat Mater*. 2021;20(10):1401–1406.
88. Wood C, Emin D. Conduction mechanism in boron carbide. *Phys Rev B*. 1984;29(8):4582.
89. Niu J, Lu N, Li L, Liu M. Polaron effect dependence of thermopower in organic semiconductors. *Phys Lett A*. 2014;378(48):3579–3581.
90. Vázquez JL. *The porous medium equation: Mathematical theory*. Oxford (UK): Oxford University Press; 2007.
91. Ni M, Leung MK, Leung DY, Sumathy K. An analytical study of the porosity effect on dye-sensitized solar cell performance. *Sol Energy Mater Sol Cells*. 2006;90(9):1331–1344.
92. Anta JA, Casanueva F, Oskam G. A numerical model for charge transport and recombination in dye-sensitized solar cells. *J Phys Chem B*. 2006;110(11):5372–5378.
93. Maldon B, Thamwattana N. Review of diffusion models for charge-carrier densities in dye-sensitized solar cells. *J Phys Commun*. 2020;4(8):Article 082001.
94. Suwardi A, Bash D, Ng HK, Gomez JR, Repaka DM, Kumar P, Hippalgaonkar K. Inertial effective mass as an effective descriptor for thermoelectrics via data-driven evaluation. *J Mater Chem A*. 2019;7(41):23762–23769.
95. Wang X, Wang W, Yang C, Han D, Fan H, Zhang J. Thermal transport in organic semiconductors. *J Appl Phys*. 2021;130(17):Article 170902.
96. Kiefer D, Yu L, Fransson E, Gómez A, Primetzhofer D, Amassian A, Campoy-Quiles M, Müller C. A solution-doped polymer semiconductor:insulator blend for thermoelectrics. *Adv Sci*. 2017;4(1):1600203.
97. Zapata-Arteaga O, Perevedentsev A, Marina S, Martin J, Reparaz JS, Campoy-Quiles M. Reduction of the lattice thermal conductivity of polymer semiconductors by molecular doping. *ACS Energy Lett*. 2020;5(9):2972–2978.
98. Weathers A, Khan ZU, Brooke R, Evans D, Pettes MT, Andreasen JW, Crispin X, Shi L. Significant electronic thermal transport in the conducting polymer poly(3,4-ethylenedioxythiophene). *Adv Mater*. 2015;27:2101–2106.
99. Scheunemann D, Kemerink M. Non-Wiedemann-Franz behavior of the thermal conductivity of organic semiconductors. *Phys Rev B*. 2020;101(7):Article 075206.
100. Liu J, van der Zee B, Alessandri R, Sami S, Dong J, Nugraha MI, Barker AJ, Rousseva S, Qiu L, Qiu X, et al. N-type organic thermoelectrics: Demonstration of ZT > 0.3. *Nat Commun*. 2020;11(1):5694.
101. Bubnova O, Khan ZU, Malti A, Braun S, Fahlman M, Berggren M, Crispin X. Optimization of the thermoelectric figure of merit in the conducting polymer poly(3,4-ethylenedioxythiophene). *Nat Mater*. 2011;10(6):429–433.
102. Huewe F, Steeger A, Kostova K, Burroughs L, Bauer I, Strohriegl P, Dimitrov V, Woodward S, Pflaum J. Low-cost and sustainable organic thermoelectrics based on low-dimensional molecular metals. *Adv Mater*. 2017;29(13):1605682.
103. Pudzs K, Vembris A, Rutkis M, Woodward S. Thin film organic thermoelectric generator based on tetrathiotetracene. *Adv Electron Mater*. 2017;3(2):1600429.
104. Sanduleac I, Pflaum J, Casian A. Thermoelectric properties improvement in quasi-one-dimensional organic crystals. *J Appl Phys*. 2019;126(17):Article 175501.
105. Brunetti I, Dash A, Scheunemann D, Kemerink M. Is the field of organic thermoelectrics stuck? *J Mater Res*. 2024;39(8):1197.
106. Dash A, Guchait S, Scheunemann D, Vijayakumar V, Leclerc N, Brinkmann M, Kemerink M. Spontaneous modulation doping in semi-crystalline conjugated polymers leads to high conductivity at low doping concentration. *Adv Mater*. 2024;36(13):2311303.
107. Persson G, Järsvall E, Röding M, Kroon R, Zhang Y, Barlow S, Marder SR, Müller C, Olsson E. Visualisation of individual dopants in a conjugated polymer: Sub-nanometre 3D spatial distribution and correlation with electrical properties. *Nanoscale*. 2022;14(41):15404–15413.
108. Wang D, Ding J, Ma Y, Xu C, Li Z, Zhang X, Zhao Y, Zhao Y, Di Y, Liu L, et al. Multi-heterojunctioned plastics with high thermoelectric figure of merit. *Nature*. 2024;632(8025): 528–535.
109. Ulrich G, Pfitzner E, Hoehl A, Liao J-W, Zadvorna O, Schweicher G, Sirringhaus H, Heberle J, Kästner B, Wunderlich J, et al. Thermoelectric nanospectroscopy for the imaging of molecular fingerprints. *Nano*. 2020;9(14): 4347–4354.
110. Nikiforov GO, Venkateshvaran D, Mooser S, Meneau A, Strobel T, Kronemeijer A, Jiang L, Lee MJ, Sirringhaus H. Current-induced joule heating and electrical field effects in low temperature measurements on TIPS pentacene thin film transistors. *Adv Electron Mater*. 2016;2(12):1600163.